Atmospheric aerosol optical properties and radiative forcing over two metros in South Africa

Abdulaziz Tunde Yakubu[1] and Naven Chetty[1]

[1]University of KwaZulu-Natal

September 11, 2023

Abstract

Aerosol Robotic Network (AERONET) measurement data is used in the validation of two prominent satellite aerosol property retrieval, Multiangle Imaging Spectroradiometer (MISR) and Moderate Resolution Imaging Spectroradiometer (MODIS), then applied to examine the properties of aerosols and the direct influence on radiative forcing (RF) over two metropolitan cities, Cape Town (CPT) and Pretoria (PRT) in South Africa. The synoptic characteristics of aerosols over CPT for 2015-2019 indicate a general low aerosol optical depth (AOD) of an average of 0.08 ± 0.014 and are prevalently sea salt (SS) aerosols. In contrast, a high AOD value with an average of 0.23 ± 0.050 was observed over PRT between 2011-2019 and predominated by sulphate/nitrate aerosols. These two dominant aerosol types are found to be the primary motivator of the net cooling effect of RF due to aerosol in each location. While the average RF over CPT is -16.79 ± 5.61 during the study period, the value over PRT is estimated to be more than two times (-36.55 ± 10.54) of the former. The validation of MISR and MODIS satellite aerosol properties retrieval for the region demonstrated better accuracy over the land than in the maritime environment. Meanwhile, MODIS underestimated AOD by [?] 32% but generally reported better precision across the board than the MISR instrument. Further investigation into the seasonal variation of aerosols over the two locations identified seasonality changes in the characteristics of aerosols mainly influenced by the transport of high-absorbing biomass-burning aerosols.

Atmospheric aerosol optical properties and radiative forcing over two metros in South Africa

Abdulaziz T. Yakubu[1], and Naven Chetty[1]

[1]Discipline of Physics, School of Chemistry and Physics, University of KwaZulu-Natal, Pietermaritzburg, 3209, South Africa

Key Points:

- The radiative forcing over South Africa is a net negative effect mainly associated with sea salt aerosol in the south and sulphate/nitrate aerosol in the north.
- A seasonal drift in absorbing aerosol concentration is observed from north to south and often influences aerosol suspension's optical and spectral characteristics over the region leading to decreasing cooling effect.
- The satellite retrieval over South Africa demonstrated significant agreement with AERONET measurements and mainly over the land than the water.

Corresponding author: Naven Chetty, `chettyn3@ukzn.ac.za`

Abstract

Aerosol Robotic Network (AERONET) measurement data is used in the validation of two prominent satellite aerosol property retrieval, Multiangle Imaging Spectroradiometer (MISR) and Moderate Resolution Imaging Spectroradiometer (MODIS), then applied to examine the properties of aerosols and the direct influence on radiative forcing (RF) over two metropolitan cities, Cape Town (CPT) and Pretoria (PRT) in South Africa. The synoptic characteristics of aerosols over CPT for 2015-2019 indicate a general low aerosol optical depth (AOD) of an average of 0.08 $\pm$ 0.014 and are prevalently sea salt (SS) aerosols. In contrast, a high AOD value with an average of 0.23 $\pm$ 0.050 was observed over PRT between 2011-2019 and predominated by sulphate/nitrate aerosols. These two dominant aerosol types are found to be the primary motivator of the net cooling effect of RF due to aerosol in each location. While the average RF over CPT is -16.79 $\pm$ 5.61 during the study period, the value over PRT is estimated to be more than two times (-36.55 $\pm$ 10.54) of the former. The validation of MISR and MODIS satellite aerosol properties retrieval for the region demonstrated better accuracy over the land than in the maritime environment. Meanwhile, MODIS underestimated AOD by $\approx$ 32% but generally reported better precision across the board than the MISR instrument. Further investigation into the seasonal variation of aerosols over the two locations identified seasonality changes in the characteristics of aerosols mainly influenced by the transport of high-absorbing biomass-burning aerosols.

Plain Language Summary

Air pollutants from human and natural resources often modify the amount of energy reaching the earths surface from the sun. Over South Africa, an enhanced cooling effect is often experienced due to the predominantly scattering characteristics of suspended particles. However, occasionally induced absorbing pollutants from the northern part of the region diffused southward and changed the atmospheric characteristics of the area. The extent of influence over parts of the region significantly depends on the proximity to the prime aerosol sources.

1 Introduction

Atmospheric aerosols are known to influence global weather and climate conditions. However, the extent of this influence solely and relative to other components that impact observable changes in the weather and climate system forms a significant source of ambiguity (Boucher, 2015; IPCC, 2013). Aerosol particles significantly interact with incoming solar radiation directly through scattering and absorption and indirectly by modifying the clouds microphysical properties (Haywood & Boucher, 2000) while serving as cloud condensation and ice nuclei (CCN and IN) during cloud formation (Ackerman et al., 2000; Twomey, 1977). Also, they interact with terrestrial (longwave) radiation via absorption and re-emission to alter the amount of outgoing electromagnetic radiation (Hansen et al., 1997). The interaction of these particles with solar as the primary energy source and terrestrial radiations results in the earths energy budget perturbation, which often drives the changes in weather and climate conditions (Hansen et al., 1997; Haywood & Boucher, 2000). More so, aerosols influence differing atmospheric and environmental challenges ranging from poor air quality, health problems, low visibility, and a dusty environment (Falaiye et al., 2013; Pope et al., 2002; Putaud, 2010) which are detrimental to human survival and general well-being. In contrast, aerosols are vital components of cloud formation and rainfall and sometimes serve as an essential source of soil nutrients favourable to humans (Falaiye et al., 2013; Fan et al., 2016). Therefore, regular qualitative and quantitative assessments are crucial for properly managing its consequences regarding their impacts on the earths energy budget and humans.

Aerosols are emitted from different sources, vary in types and properties, and the distribution is susceptible to spatio-temporal changes (Yakubu & Chetty, 2020). Furthermore, based on the listed characteristics, aerosol particles influence the earth and its atmosphere to varying degrees on a regional and global scale (IPCC, 2013). However, due to the poor understanding of how different aerosol characteristics translate to differing atmospheric and climate changes, their impacts are associated with significant uncertainty (IPCC, 2013; Jacobson, 2001). Similarly, the knowledge and uncertainty gaps in characterising and quantifying aerosol effects result in their underrepresentation in the cloud and the general circulation model (GCM) (Gettelman & Sherwood, 2016; Seinfeld et al., 2016). Therefore, proper quantification of the variation and roles of different aerosol types become critical in characterising their corresponding effects efficiently.

Over the years, various approaches have been employed to measure and determine aerosol characteristics, including in-situ measurement, ground and satellite remote sensing, and modelling (de Meij & Lelieveld, 2011; Drury et al., 2008; Dubovik & King, 2000). Each process has distinct drawbacks ranging from poor spatial coverage to temporal instability and low sensitivity. In-situ or field campaigns are the most accurate aerosol monitoring method but are significantly disadvantaged by the limited spatiotemporal range (Formenti et al., 2002; Ichoku et al., 2003; Smirnov et al., 2003). Meanwhile, in practice, remote sensing from both ground and satellite platforms constitutes the most commonly used method of aerosol measurement (Yakubu & Chetty, 2020). These methods are mainly advantageous due to their effectiveness in measuring the total column values of aerosol and non-intrusiveness (Smirnov et al., 2002). Besides, they possess considerably high stability in terms of temporal and spatial coverage. Although ground observation is still considered among the most effective remote form of observing aerosol properties. They are yet faced with the limitation of poor spatial coverage. Satellite-measured aerosol properties are less efficient, though they possess an uninterrupted temporal and broader spatial range (Sherman et al., 2016; Yakubu & Chetty, 2020). Therefore, ground and satellite remote sensing synergy for aerosol monitoring has demonstrated promising results (Kaufman et al., 2000). Also, modelled generated aerosol data is similarly stable temporally and spatially but prone to several errors since such data depends on in-situ, ground, and satellite data. Applying any or the synergy of these methods has helped characterised aerosol and investigate its impacts on climate (Schuster et al., 2012; Sherman et al., 2016; Yakubu & Chetty, 2020).

Natural and anthropogenic aerosols are often found as a mix globally. However, several studies have suggested that the increase in anthropogenic aerosols leads to the current challenge posed by climatic change (Charlson et al., 1992; IPCC, 2013; Schwartz et al., 2002). Also, findings have demonstrated that the aerosol suspension over an area is a function of both localised generated and in-ward transported aerosols from the external origin (Yakubu & Chetty, 2020). Hence, the characteristics of aerosol suspension can be predominantly influenced by localised generated aerosols or influx of transported aerosol particles. Meanwhile, some studies have shown that internally generated aerosols that mainly form a canopy over urban/industrialised environments emerge primarily from anthropogenic sources (Charlson et al., 1992; Schwartz et al., 2002; Wang et al., 2018). However, the occasional influx of transported aerosols also increases the aerosol suspended in some cases.

In contrast, rural and semi-urban areas are commonly dominated by natural aerosol emission but occasionally experience a sharp increment in aerosol suspension mainly due to the influx of transported particles (IPCC, 2007; Smirnov et al., 2003). Also, the mix of different aerosol suspensions has differing impacts on the corresponding region. Studies from various parts of the world have shown fine mode particles with generally absorbing characteristics and mainly originating from anthropogenic sources dominate the urban/industrial environments (IPCC, 2013; Yakubu & Chetty, 2020). The typical impact associated with this aerosol environment is an increase or decrease in the radiative forc-

ing (Twomey, 1977; Wang et al., 2018) due to the absorbing or scattering nature of the predominant particles, depending on the composition of the suspended aerosols.

Studies on urban/industrial regions such as America (Smirnov et al., 2003), Europe (Putaud, 2010; Sayer et al., 2014) and Central Asia (Wang et al., 2018) have shown that the impact of suspension due to urban/industrial aerosols on radiative forcing is a net warming effect (positive RF) following the strong absorption features of the constituents. Meanwhile, related studies in a similar setting elsewhere have shown the reverse (Yun et al., 2022). Polluted environments have also been presented to suppress precipitation formation (Fan et al., 2016; Rosenfeld, 1999). Nevertheless, some studies have found precipitation enhancement by high aerosol loading (Christensen & Stephens, 2012; Fan et al., 2016). Studies have consistently explained the two situations mainly to be influenced by atmospheric dynamics and thermodynamics (Fan et al., 2016; Rosenfeld et al., 2014). Over South Africa (SA), some studies have been carried out on characterising atmospheric aerosols suspended in the region. These include aerosol optical properties, the effect on radiative forcing, impacts on cloud and precipitation, and air pollution (Adesina et al., 2016; Formenti et al., 2002; Hersey et al., 2015; Ichoku et al., 2003). Generally, from those investigations, aerosols over SA exhibit seasonality centred around spring and aerosol loading is highest in the upper parts compared to the lower areas (Adesina et al., 2016; Tesfaye et al., 2011; Yakubu & Chetty, 2020).

Similarly, these studies have shown that the upper parts are distinctly dominated by fine mode aerosol, while the lower parts are a mix of coarse and fine aerosols. The primary sources of aerosols identified by these studies are observed to depend on the level of industrialisation, population and other related human activities. Also, they are sometimes enhanced by seasonal influx of biomass burning aerosol from neighbouring communities.

Regarding spatial coverage, most studies have investigated aerosol activities in fewer locations based on ground data, such as AERONET (Kumar et al., 2017; Queface et al., 2011) and more multilocation studies using satellite instruments data (Adesina et al., 2016; Tesfaye et al., 2011). Meanwhile, the validation of satellite aerosol retrieval over SA remains minimal, and most studies conducted using ground instruments such as sun photometers are mainly single location-based observations. Hence, only a few studies (Hersey et al., 2015; Yakubu & Chetty, 2020) have examined the validation of satellite measurements over the region, which are limited to small spatial coverage and often involve selected parameters. With the growing industrialisation and population across the region, urban expansion calls for more climate actions. Hence, understanding aerosol properties and the accompanying impacts become essential. Besides, more studies are needed to validate satellite-retrieved and modelled generated data, considering the vast gap set by satellite-based predominated studies over the region. This approach will enhance the reliability of satellite-based observations in studying aerosol regionally and globally.

This work investigates aerosol optical characteristics and the consequential impacts on radiative forcing over two metropolises in South Africa with distinct industrial and population footprints. Each of the two study areas represents the upper and lower parts of the country, respectively, and is strategic to Southern Africa. Furthermore, the areas are host to AERONET sun photometers and boast relatively consistent data regarding availability amongst peers. The study explores the advantages of these two sites attributes (as mentioned above) to understand the aerosol characteristics and radiative effects of locally generated and inward-transported aerosols. The role of naturally emitted and anthropogenic aerosols over each environment and proxy location is examined. Equally important, data from two satellite instruments over the sites will be validated using the AERONET data. The results present a comprehensive insight into identifying the predominant types and sources of aerosols in South Africa and their effects on the region. Further, the study will assist in deciding on an appropriate measure to tackle the climate change issue. Also, this output portrays a significant advance towards optimising satellite retrieval of aerosol

measurements over Africa and enhancing the modelling of aerosols over the region. Subsequently, section two describes the data, sources, and general approach to this study. Sections three and four give the study's detailed results and general discussion. Finally, the summary and a brief conclusion of the outcomes of this work are presented in section five.

2 Data and Methods

2.1 Locations

This study focused on two strategic metros (Pretoria and Cape Town) in South Africa (SA), separated by ≈ 2000 km within the regions geographical space (see Figure 1). Cape Town (33.92° S, 18.42° E) is one of the largest metropolitan areas in SA, located in the southernmost and coastal part of the region. The area has a mountainous and hilly landscape, including the famous Table Mountain, a popular tourist site. Also, the environment is typically a marine environment due to the nearness to the coast of SA. Cape Town is home to several industrial and commercial activities and represents the economic centre of the Western Cape province. The area, with a population of over 2-million people, is involved in different light industrial and domestic activities that result in the emission of a considerable amount of aerosols. Aerosols such as SO_4, NO_3, black (BC) and organic carbons (OC) are typical of this location (Yakubu & Chetty, 2020). Some aerosol impacts in this area include increased air pollution, weather changes, and associated health implications. Between 2013 and 2015, the region experienced low rainfall and was potentially prone to drought (Yakubu & Chetty, 2020). Similarly, a slight rise in air pollution and poorer air quality are observed from 2014 to 2018 (Yakubu & Chetty, 2022, 2020).

Pretoria (25.75° S, 28.28° E) is in Gauteng province northeast of SA, with another metropolis, Johannesburg, known as the country's economic capital. Due to proximity, the neighbouring city's (i.e., Johannesburg) population and activities significantly influence this area. Pretoria, popularly known as the administrative domain of SA, is home to extensive industrial activities, particularly the heavy steel industries. Mining activities and the coal power plant around the area are also essential sources of aerosol emission. In the last two decades, the city has suffered climate change impacts such as heat waves, precipitation drops and drought (McBride et al., 2022; Sen Roy & Rouault, 2013). Considering the series of climate change related events observed in the environment, there is a need to understand the role of aerosol emission changes over the area to mitigate the possible re-occurrence of such negative influences effectively. Besides, this study will enhance the characterisation of aerosols regionally and globally.

2.2 Data

For a detailed understanding of the aerosol properties and their corresponding impacts, this study utilises data from ground and satellite platforms to arrive at the result presented. The ground observation data is from the AERONET (Aerosol Robotic Network) stations in both locations. AERONET is a ground-based network of sun photometers that monitors the near real-time global distribution of aerosol spectral optical thickness through direct sun collimated and sky radiance measurements. The radiometers within the network take measurements at eight spectral bands: 340 nm, 440 nm, 500 nm, 675 nm, 870 nm, 970 nm and 1020 nm. The direct sun radiation is measured in all eight spectra, while the sky radiation is obtained at four wavelengths (440 nm, 670 nm, 870 nm and 1020 nm). Furthermore, AERONET provides aerosol optical depth (AOD) measurement at seven spectral bands and a nominal uncertainty of ≈ ±0.01-0.02 (Eck et al., 2013; Holben et al., 1998). From the AOD measurements at two reference wavelengths, another vital parameter, the Angstrom exponent (AE or α), which gives insight into the size characteristics of aerosols, is obtained. Also, from the spectral deconvolution algo-

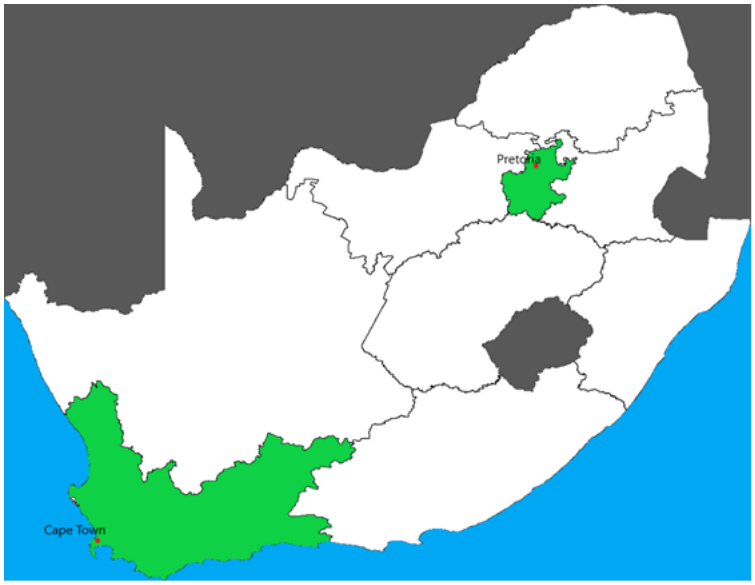

Figure 1. The map of South Africa showing the locations of Cape Town and Pretoria

rithm (SDA), properties such as the fine mode fraction (FMF) and AOD (τ_f) are inferred using the instrument measurements. Apart from the optical parameters, the network of radiometers produces microphysical parameters, including the volume size distribution, single scattering albedo (SSA), refractive indices (RI), and absorbing AOD (τ_{abs}), amongst others, using the flexible inversion algorithm and the sky radiance measurement as input (Dubovik & King, 2000). Several works have documented a detailed description of the retrieval method and products following the flexible inversion algorithm (Dubovik & King, 2000; Yakubu & Chetty, 2020). In this work, the level 1.5 scientific datasets from AERONET measurements for Pretoria and Simons Town sites to present the results herein. The preference for level 1.5 (cloud screen only) over level 2.0 (cloud screen and quality assurance) datasets is due to the size of datasets offered by the former and the consistency ($> 90\%$) compared to the latter, as observed from the two sites. Generally, the AERONET data is vital to this study as it provides an insightful view of aerosol optical and microphysical properties over the locations and validates satellite-derived data.

Both satellite data used in this study are measurements obtained from two instruments on board the Terra satellite, one of the A-train constellation satellites. The multiangle imaging spectroradiometer (MISR) instrument measures the reflected solar radiation from the earths surface by nine different cameras positioned at different angles; nadir, $\pm$ 26.1°, $\pm$ 45.6°, $\pm$ 60.0° and $\pm$ 70.5°, to monitor changes in global climate. Each of the nine cameras operates at four wavelengths; blue (443 nm), green (555 nm), red (670 nm) and infrared (865 nm) to provide various scientific datasets on aerosol and cloud properties beneficial for the proper characterisation of their impact on global climate. MISR possess the advantage of being carefully calibrated to operate at optimal accuracy to provide data at a high spatial resolution (Abdou et al., 2005; Diner et al., 1998; Kahn et al., 2010). Besides, the instrument offers the classification of aerosol particle size distribution among its peers. In the present study, level-3 daytime daily and monthly data at a spatial resolution of 0.5° x 0.5° are utilised to present additional results.

The moderate resolution imaging spectroradiometer (MODIS) has radiometric capabilities to measure the reflectance from clouds and the earths surface at 36 different spectrums ranging from visible to infrared. The instrument monitors the activities of aerosol and clouds at a horizontal resolution between 250 m and 1 km. MODIS produces different levels of aerosol products ranging from raw data (Level 1) to more refined datasets (Level 2 to Level 4). The higher-level aerosol products generally pass through further processing, where the datasets undergo different screening algorithms designated to filter-off inconsistent data. Also, a quality assurance (QA) flag is associated with successive product levels to enhance the quality of interpretation. Datasets from MODIS instruments form the basis of several studies, particularly over vast areas with no ground instruments. Hence, it is crucial to validate the data available from this instrument over all possible locations to assess the credibility in evaluating the past, present and future states of the atmosphere. Daily and monthly standard level 3, 1° x 1° gridded datasets are used for the analysis presented in this paper.

To evaluate the validation of the satellite retrieved data against the AERONET ground observation data, statistical metrics to include the correlation coefficient (R-value), significance value via 2-tail test (P-value), root mean square error (RMSE), mean average error (MAE) and the percentage mean bias (PMB) are considered. The identifications of the dominant aerosol types follow the application of an unsupervised clustering machine learning algorithm deployed using the Python Scikit module to corroborate the traditional identification process based on aerosol characteristics. Quantifying the direct radiative forcing (RF) due to aerosol in this work is based on the radiative transfer model. This model considers the difference in net fluxes (i.e., upward and downward fluxes) due to aerosol (without cloud) to estimate the RF at the top (TOA) and bottom (BOA) of the atmosphere. Thus, the average RF (ARF) over a region is typically esti-

mated as a function of RF at TOA and BOA following the expression below (Boiyo et al., 2019; Kumar et al., 2017);

$$ARF = RF_{TOA} - RF_{BOA}, \tag{1}$$

where,

RF_{TOA} = radiative forcing at the top of atmosphere

RF_{BOA} = radiative forcing at the bottom of atmosphere.

For this study, the RF at TOA ($RF^{'}_{TOA}$) and BOA ($RF^{'}_{BOA}$) derived from AERONET radiative forcing products are used. While the AERONET inferred $RF^{'}_{TOA}$ is used directly in equation (1) to account for net flux at TOA (i.e., $RF^{'}_{TOA}$= RF_{TOA}), $RF^{'}_{BOA}$ is applied to account for the downward net flux only. So, to represent the complete forcing at BOA to cater for the upward net flux, a correctional term as a function of the surface albedo ($\omega^{'}$) is applied to $RF^{'}_{BOA}$. Thus, RF_{BOA} in equation (1) is then expressed as;

$$RF_{BOA} = (1 - \omega^{'})RF^{'}_{BOA}. \tag{2}$$

Based on equation (2), the estimation of $\omega^{'}$ is done through the dataset of the MODIS albedo products. Thus, the level-3 MCD43A3 and the corresponding quality product (MCD43A1) are utilised to derive $\omega^{'}$ at the zenith ranging from 40° - 80° to account for changes in the instantaneous albedos (Wang et al., 2015).

3 Results

3.1 Aerosol optical properties statistics

The monthly averages of the parameters AOD, AE, FMF, AOD_{abs}, SSA and WVC over the study period 2015-2019 for Cape Town (CPT) and 2011-2019 for Pretoria (PRT) are presented in Figures 2 and 3. Generally, aerosol loading measured by AOD is lower in CPT (AOD_{av_440} = 0.08 ± 0.014), typical of the maritime environment (Smirnov et al., 2003), compared to PRT (0.23 ± 0.050), which boasts of more industrial activities, especially in the heavy metal industries. These observed values agree well with the reported ones from previous studies (Kumar et al., 2017; Yakubu & Chetty, 2020). Also, noticeably the two locations differ in the period of min-max occurrence of aerosol loading due to slight differences in climate patterns. Remarkably, the meteorological states are critical to aerosol characterisation owing to their roles in suspension and removal from the atmosphere. For instance, CPT is associated with the winter rainfall season resulting in the increase in aerosol removal by scavenging clouds ahead of the rainy events and is suggestively accountable for the minimum AOD (0.060) in April, as shown in Figure 2a, while the continuous suspension and the influx of air masses carrying aerosol is linked to maximum AOD (0.103) in August and most parts of spring.

Meanwhile, the case slightly differs for Pretoria, as illustrated by Figure 2b, such that the minimum AOD (0.159) occurred in June and the maximum (0.341) in September, extending through the spring season as seen for CPT and often associated with the events of biomass burning (BB) during the pre-farming season. Studies have repeatedly linked the BB events accounting for the high aerosol turbidity over the two locations in spring to mainly emanate from the northern parts of South Africa and neighbouring countries (Formenti et al., 2002; Hersey et al., 2015; Hodnebrog et al., 2016; Yakubu & Chetty, 2020). The concentration over each site is a function of the proximity and wind flux towards the area.

Following the characteristic aerosol loading over the study sites, CPT demonstrated the predominance of coarse particles (i.e., AE < 1.0) with a multiyear monthly average of 0.733 ± 0.128. At the same time, PRT tends more toward fine mode aerosols (i.e., AE > 1.0) with an average AE value of 1.517 ± 0.072. From Figure 2c, the minimum monthly mean AE (0.504 in March) and generally lower AE over Cape Town occur during the summer and autumn and coincide with the reduced influx of transported aerosol over the site. This variation significantly portrays the feature of a typical less polluted maritime environment with the predominance of sea salt (SS) aerosol. Previous studies over similar sites (de Leeuw et al., 2011; Smirnov et al., 2003), including this current site (Yakubu & Chetty, 2020), have demonstrated comparable variation and have been linked to a pristine coastal area predominated by coarse aerosol of SS origin. Similarly, the maximum monthly mean (0.929 in September) represents increasing aerosol loading dominated by finer particles and corresponds to the period of high atmospheric turbidity. This variation is associated mainly with the spring months, typically characterised by (internal and external) biomass burning and fossil fuel combustion. In contrast, aerosol suspension over Pretoria is chiefly dominated by fine mode aerosols (see Figure 2d). A mean monthly average AE (1.52) is recorded over PRT during the study period. Emissions from industrial activities, vehicular movements and other domestic activities are more likely to account for this variation. Meanwhile, the minimum AE (1.409 in July) and during the entire winter months suggest a decrease in fine particle dominated aerosols, such as BB aerosol, by relatively considering the drop in AOD value. The maximum (AE = 1.597 in December) and generally from spring to autumn indicates the enhanced emission and suspension of fine mode particles, influenced by the BB aerosol influx from external sources. This AE characteristic over PRT is consistent with the observation from a previous study over the site (Kumar et al., 2017).

The FMF variation from the spectral deconvolution algorithm (SDA) is presented in Figures 2e and 2f (i.e., for CPT and PRT, respectively) further to examine the particle size characteristics over the study sites. Coarse mode dominates atmospheric aerosol suspension over CPT, with FMF mostly less than 0.5 during most months of each season, such that the monthly average value (0.45 ± 0.056) reflects the dominance. This observation, coupled with the AOD and AE variation earlier described, strongly suggest SS as the primary aerosol type over the region. The minimum average FMF (0.360 in March) and low values in most months further display the strong dominance of SS aerosol over the area and less pollution. The maximum mean (0.542 in September) and relatively high values during winter signify increased pollution. These observations considerably align with the earlier findings in this work and the hypothesis from a previous study (Yakubu & Chetty, 2020), noting the influx of polluted air mass mainly linked to BB aerosol (i.e., aged smoke) from the northern part of South Africa. In contrast, FMF variation over PRT of a monthly mean value of 0.780 ± 0.029 illustrates the predominance of fine mode aerosol in the site. The minimum FMF (0.730 in November) represent the period of less influx of external air pollutant (especially aged smoke), while the maximum (0.821 in September) demonstrates the enhancement of internal air pollution due to the external influx of aerosol particles.

Figures 3a and 3b illustrate the variation of absorbing AOD (AOD_{abs} or τ_{abs}) over Cape Town and Pretoria, respectively. AOD_{abs} also constitute a vital property in aerosol characterisation and enhance the identification of different aerosol types. Aerosols such as carbon soot (CS) and black carbon (BC) are strong absorbers of solar radiation, hence, identifiable by high τ_{abs}. Low or relatively moderate τ_{abs} can infer moderately absorbing aerosols such as organic carbon (OC) and MD; those with poor absorbing properties are differentiable by extremely low AOD_{abs}. On this note, τ_{abs} is generally low over CPT (mean $\tau_{abs} = 0.005 \pm 0.002$) compared to PRT (mean $\tau_{abs} = 0.019 \pm 0.009$) with $\approx$ 4-times absorbing characteristics of CPT. The features presented by the AOD_{abs} variations in the two locations support the pattern demonstrated by AOD, AE and FMF. Also, the differences in τ_{abs} between the two sites beam more insight into the role of prox-

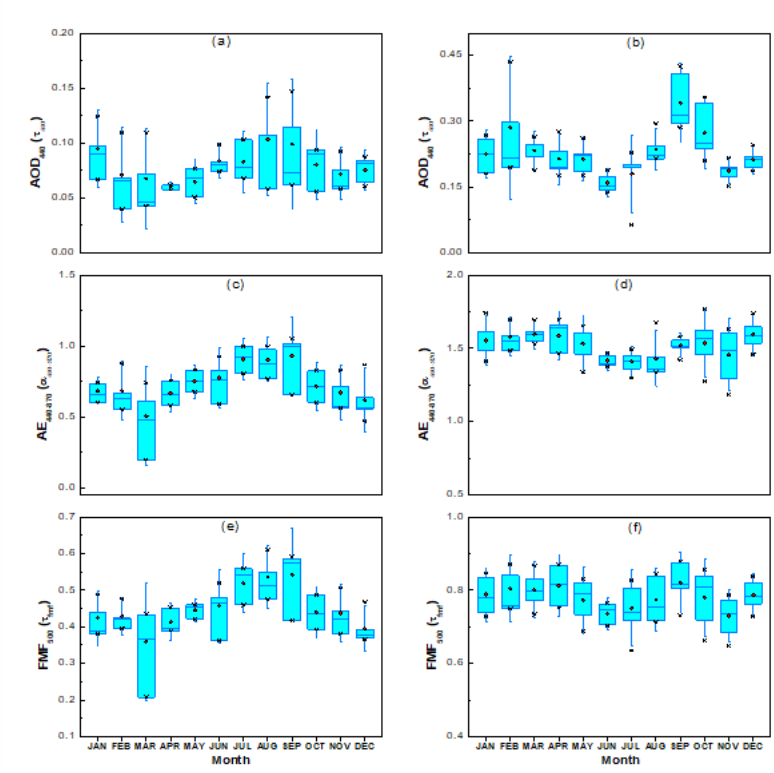

Figure 2. The graphs of the multiyear monthly mean AOD, AE and FMF for Cape Town; (a), (c) and (e), and Pretoria; (b), (d) and (f)

imity in the aerosol characteristics over each location. PRT is closer to the prime source of BB aerosols resulting in higher τ_{abs}, while CPT further away from the origin accounts for the lesser τ_{abs}.

Similar but opposite to τ_{abs}, the single scattering albedo (SSA or ω) variation over the study locations is described in Figures 3c and 3d for CPT and PRT, respectively. Over CPT, the monthly mean ω value is 0.932 ± 0.022 suggesting a considerable dominance of scattering suspensions. Factoring the variations portrayed by AOD, AE, FMF, and AOD_{abs}, the assertion of SS aerosols matching the predominant aerosol type over the Cape Town site is more apparent. The finding is consistent with the previous studies on the location (Yakubu & Chetty, 2020). Nevertheless, it is essential to note from the min-max SSA (i.e., 0.897-0.967) that aerosol suspended over this site sometime constitutes the mix of coarse-fine mode particles leading to characteristics shift in the value of SSA from strong to less scattering. Internal emissions such as domestic and industrial emissions and the influx of aged smoke-bearing air masses are often liable to these changes.

Similarly, the monthly mean ω in PRT is 0.899 ± 0.027, which chiefly represents scattering aerosols. However, compared with the obtained value over CPT, it demonstrates a more absorbing trait typical of an urban-industrial location and its proxy to the primary BB sources. The minimum average SSA (0.860) occurs in August, and the maximum value (0.948) is recorded in December. The minimum SSA and other lower values ($\omega < 0.890$) are chiefly associated with the winter and spring months, coinciding with the pre-planting period in South Africa and bordering countries. From the variations of SSA and other aerosol properties over Pretoria, one can observe the dominance of less absorbing and more scattering particles (like sulphate and nitrate aerosols) during autumn and summer. Likewise, the influence of less scattering and more absorbing aerosols (e.g., black and organic carbon) is observable around the winter and spring, thereby changing the spectral properties of the suspended particles.

Figures 3e and 3f illustrate the variations of atmospheric water vapour content (WVC) for CPT and PRT. WVC or precipitable water for both locations are similar in interpretation such that atmospheric vapour is lowest during winter (i.e., CPT;1.17 cm and PRT;0.67 cm, both in July) and highest in summer (CPT;1.99 cm in January and PRT;2.05 cm in December). This pattern is typical for all parts of South Africa, where WVC is all high during summer and lowest in winter. The monthly average WVC for the sites is 1.52 ± 0.29 cm and 1.35 ± 0.54 cm for Cape Town and Pretoria, respectively. Notably, the average WVC over CPT is higher than the value for PRT and is link-able to the nearness to the ocean since air temperature over the water drops slower compared to the land. Generally, the characteristics of high WVC during summer have been consistently reported over the hemispheres (Sioris et al., 2016; Yakubu & Chetty, 2022). Hence, the finding in this study is in good agreement with past studies.

Figures 4 and 5 show the validation of aerosol optical parameters data from the satellite (i.e., MISR and MODIS) observations over the locations under investigation against AERONET ground-measured data. In figures 4a and 4b representing Cape Towns MISR and MODIS AOD validations, respectively, one can see that the latter demonstrated better agreement with AERONET AOD following a moderate relationship (i.e., $R = 0.561$; $P << 0.001$) compared to the former with a very weak correlation (i.e., $R = 0.173$; $P = 0.466$). Also important, while MISR overestimated AOD over CPT by more than 50% relative to AERONET measurement, MODIS underestimated the parameter by approximately 10% (see Table 1 for complete metrics). Generally, both satellite instruments have been reported to retrieve AOD measurements over maritime/nearshore environments poorly (Kaufman et al., 1997). Several factors, such as the surface reflectance of water, instrument radiometric calibration, atmospheric correction and spatial resolution, are some of the sources of uncertainty in validating the two satellite instruments (Drury et al., 2008; Lora-Salazar et al., 2016). Although special algorithms are introduced in processing these datasets to correct and realign them with in-situ observation, environmen-

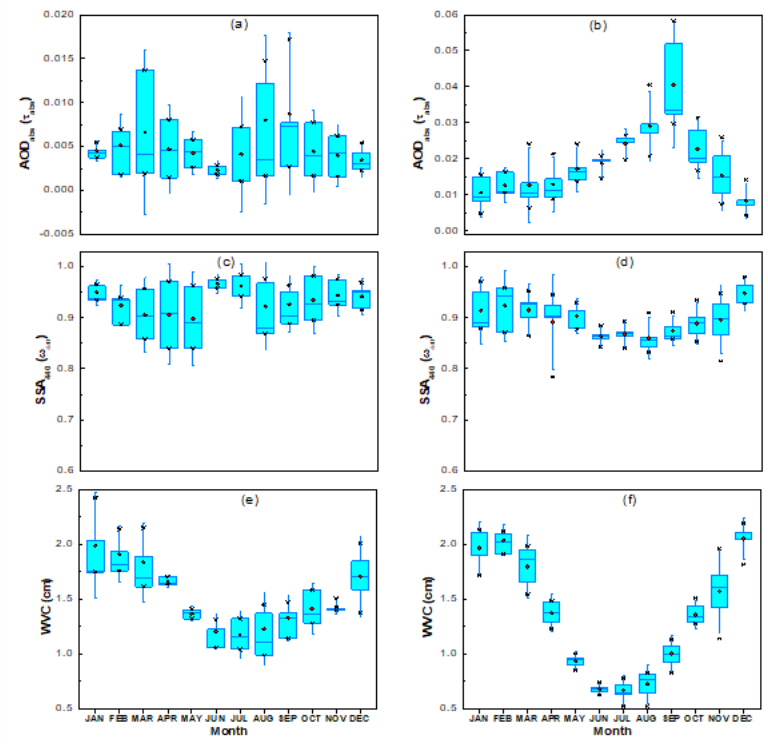

Figure 3. The plot of monthly mean AOD_{abs}, SSA_{440} and WVC for Cape Town; (a), (c) and (e), and Pretoria; (b), (d) and (f) over their respective study periods

Table 1. Summary of the statistical metrics adopted in the evaluation of the satellite validation

	CPT				
[a](M1 ; M2)	AOD	AE	AOD_{abs}	SSA	WVC
R-value	0.173 ; 0.561	0.069 ; 0.126	-0.033 ; 0.260	-0.014 ; -0.177	– ; 0.970
P-value	0.466 ; <0.001	0.773 ; 0.411	0.895 ; 0.105	0.960 ; 0.275	– ; <0.001
[b]Diff.(%)	50.08 ; -10.35	40.70 ; 103.42	13.84 ; -7.80	1.130 ; 0.590	– ; 0.570
RMSE	0.061 ; 0.026	0.380 ; 0.772	0.006 ; 0.004	0.061 ; 0.04	– ; –
MAE	0.050 ; 0.020	0.314 ; 0.753	0.005 ; 0.003	0.047 ; 0.032	– ; –
[a](M1 ; M2)	PRT				
R-value	0.611 ; 0.641	0.025 ; 0.106	0.579 ; 0.420	0.507 ; 0.424	– ; 0.990
P-value	<0.001 ; <0.001	0.858 ; 0.388	<0.001 ; <0.001	<0.001 ; 0.003	– ; <0.001
[b]Diff.(%)	-13.11 ; -53.62	-5.160 ; -1.270	-32.91 ; -58.26	3.530 ; 3.250	– ; 7.740
RMSE	0.068 ; 0.133	0.367 ; 0.133	0.011 ; 0.015	0.045 ; 0.059	– ; –
MAE	0.052 ; 0.125	0.295 ; 0.104	0.008 ; 0.012	0.037 ; 0.046	– ; –

[a]M1 = MISR, M2 = MODIS. [b]Diff.(%) = Percentage difference.

tal differences can influence the outcome of CPT. Also, the gap between the MISR and MODIS datasets is associable with the scanty data by the former compared to the latter.

Over PRT in Figures 4c and 4d, the result seems similar as seen for CPT. MODIS AOD measurement (R = 0.641; P << 0.001) slightly outperformed MISR AOD (i.e., R = 0.611; P << 0.001) in PRT. As an important note, the instruments demonstrated better retrieval on land than the ocean, as seen from observation over maritime/nearshore environments like CPT. Meanwhile, both instruments underestimated AOD relative to AERONET measurement over PRT, with MODIS taking the lead (see Table 1). Further to the above observations, improvement in data points for MISR has significantly enhanced the extent of agreement with the AERONET dataset.

AE retrievals from the two instruments relative to AERONET obtained measurements in Figures 4e 4h generally indicate weak agreements for both locations. Yet, the retrieval over the land (PRT) tends to be better than the counterpart in the nearshore CPT. In Figures 4e and 4f for CPT, MISR demonstrated a weaker correlation (i.e., R = 0.069; P = 0.773) compared to MODIS (i.e., R = 0.126; P = 0.411), respectively. Similarly, PRT in Figure 4g MISR (R = 0.025; P = 0.858) displayed a poorer correlation than MODIS (R = 0.106; P = 0.388) in Figure 4h. While both instruments averagely overestimated AE in CPT (i.e., MISR = 40.71%; MODIS = 103.42%), they underestimated the quantity in PRT (MISR = 5.16%; MODIS = 1.27%). The broader biases demonstrated by the AE retrievals are more associable with the inherited uncertainties from the AOD at individual wavelength profiled in the evaluation. Similarly, the dis-similarity in the choice of reference wavelengths in evaluating AE for the collocated AERONET and satellite instruments could also interfere with the correlation divergence.

Studying the validation plots of AOD_{abs} for the satellite instruments over CPT illustrated in Figures 5a and 5b, shows retrieval from MISR (R = -0.033; P = 0.895) and MODIS (R = 0.26; P = 0.105) weakly correlated with AERONET values. As with the observed relationship for AOD in CPT, the poor correlation was generally recorded for both satellite instruments. Nevertheless, MODIS AOD_{abs} tends to agree better with AERONET. In Figures 5c and 5d, respectively, for Pretoria MISR and MODIS AOD_{abs}, a moderate

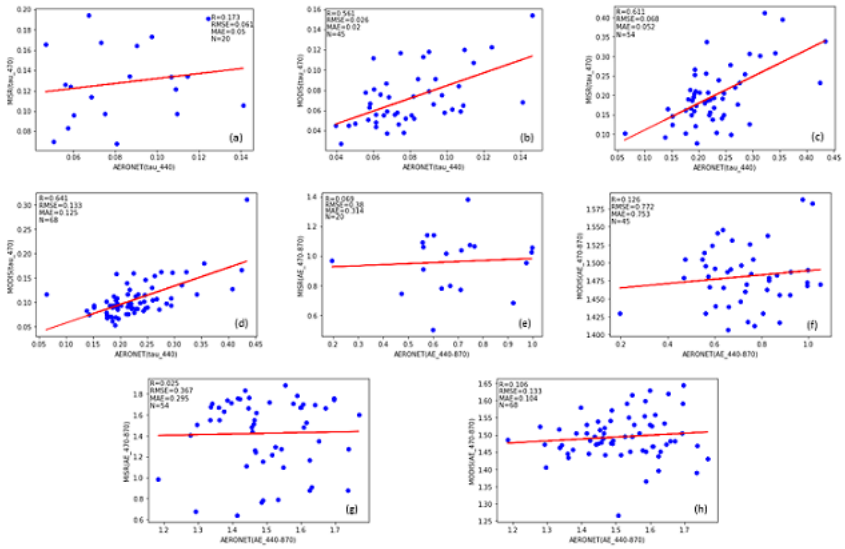

Figure 4. The plots of comparisons amongst AERONET, MISR and MODIS instrument data on AOD (a and b), AE (c and d), AOD_{abs} (e and f) and SSA (g and h) for CPT

correlation is observable for the two instruments compared to AERONET measurements. The MISR (R = 0.579; P << 0.001) demonstrated a more substantial relation with the ground instrument compared to MODIS (R = 0.42; P << 0.001). Overall, the trend of relatively better agreements of the satellite instruments with the collocated AERONET observation over the land surface is repeatedly demonstrated here for the AOD_{abs}, which is consistent with the earlier finding.

Comparison of SSA measurement between the satellites and ground instruments in Figures 5e-5h are similar to the relationship seen for AOD_{abs} over the locations. Weak connections between AERONET and the satellites SSA are recorded over CPT in which MISR (R = -0.014; P = 0.960) tends to be weaker than MODIS (R = -0.177; P = 0.275) measurement. Meanwhile, both satellite instruments posted a moderate relationship with the ground instrument in PRT, such that MODIS (R = 0.507; P << 0.001) is portrayed to be more assertive in correlation compared to MISR (R = 0.424; P = 0.003). Also essential, the satellite instruments averagely over estimated SSA measurement at both sites compared to the ground sensor, although by a minimal margin (i.e., < 4%). Further examining the satellite retrieval of another vital parameter available only from MODIS, the precipitable water, indicated robust agreement with the ground instrument in both locations. As expected, the accuracy over PRT (R = 0.99; P << 0.001) supersede that of CPT (R = 0.97; P << 0.001) and is accountable to the satellite instrument retrieval precision over land compared to the water surface. The WVC MODIS-AERONET relationship result obtained in this work consistently agrees with findings from previous studies (Kahn et al., 2010; Yakubu & Chetty, 2020, 2022).

3.2 Relationships amongst optical properties

In this section, the relationships AE vs AOD, SSA vs AOD, AE vs AOD_{abs} and aerosol index (AI) vs WVC are examined and presented in Figure 6 to further understand the aerosol characteristics over the study locations. AI represent a parameter de-

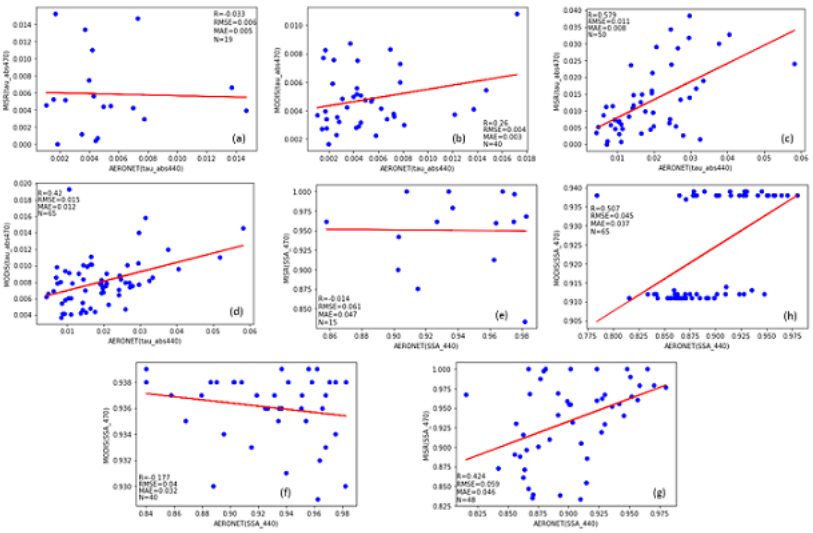

Figure 5. The plots of comparisons amongst AERONET, MISR and MODIS instrument data on AOD (a and b), AE (c and d), AOD_{abs} (e and f) and SSA (g and h) for PRT

fined as AOD *AE to factor the aerosol loading along with the size distribution in a single term. Figure 6a shows the relationship between AOD and AE for Cape Town. Mainly, low aerosol loading corresponds with large particle size (i.e., $\tau_{440} < 0.1$ primarily for $\alpha_{440-870} < 1.0$), then AOD between 0.1 and 0.15 consists of more mixed particle size (i.e., coarse and fine), and high atmospheric pollution over the location is dominated by fine-mode aerosols ($\tau_{440} > 0.15$; $\alpha_{440-870} > 1.0$). Similarly and more obviously, low aerosol loading over Pretoria is dominated by coarse-mode aerosols (i.e., $\tau_{440} < 0.1 \equiv \alpha_{440-870} < 1.0$), and high loading coincides with fine-mode particles ($\tau_{440} > 0.2 \equiv \alpha_{440-870} > 1.0$) as observed from Figure 6b.

The plot of SSA against AOD for CPT in Figure 6c demonstrates predominant scattering (i.e., $\omega > 0.9$) mainly for $\tau_{440} < 0.2$. The region of $\omega < 0.9$ coincides with $\tau_{440} > 0.2$ and the cluster of $\omega > 0.9$ lies with mostly high aerosol loading (i.e., $\tau_{440} > 0.15$). The first described region exhibits the characteristic of SS aerosols, the next is likened to carbon emission (including carbon soot, OC, and BC), and the last segment depicts sulphate and nitrate presence. These observations are consistent with the findings in the previous section and earlier study (Yakubu & Chetty, 2020), considering the environmental characteristics of CPT, such as the BB activities (including forest fire), the influx of aged smoke, and the level of industrial activities. For Pretoria in Figure 6d, again, the variation is more evident with the predominant spread of SSA > 0.9 extending from low to high aerosol loading (i.e., $0.15 < \tau_{440} < 1.20$) and the region of $\omega < 0.9$ for $0.15 < \tau_{440} < 0.90$. The first segment depicts the dominance of aerosols mostly from fossil fuel (FF) combustion (from domestic and industrial activities), such as sulphate and nitrate particles. The second part represents more mixed emissions from combustion activities (such as BB and FF) and mineral dust (MD). The characteristics of ω vs τ_{440} provide considerable evidence of CPT being SS rich, receiving low to moderate FF emissions and seasonally polluted by the combined internal and external low emissions from BB. In contrast, PRT demonstrates a significant suspension of sulphate and nitrate aerosols

through regular emissions from FF combustion and seasonally enhanced pollution by a large concentration of BB aerosol constituents (like BC, OC and soot).

The relationship between particle size and absorption strength for CPT in Figure 6e shows relatively higher τ_{abs} (> 0.02) are mainly influenced by fine-mode aerosols such as BC and OC. At the same time, the lower absorbing feature is associated with predominantly coarse mode aerosols suspected to be SS and considerable fine-mode concentration typical of FF combustion emission (sulphate and nitrate). In the case of PRT, aerosols of low absorption dominate the location. Thus, lower τ_{abs}-value mainly coincide with smaller-sized particles (AE > 1.0), and the same for $\text{AOD}_{abs} <$ with higher value ($\tau_{abs} > 0.04$). The first feature is typical of sulphate and nitrate aerosols, and the second is more of BC and soot. Meanwhile, the cluster of AE < 1.0 and $\text{AOD}_{abs} < 0.02$ comprises coarse non-absorbing aerosols, such as mainly MD considering the geographic location and the traces of SS aerosol.

Figures 6g and 6h illustrate the variation of AI with WVC for CPT and PRT. For CPT, increasing vapour content is accompanied by a moderate rise in the AI, especially for WVC values in the 1 to 2.5 cm range, which suggests growth in particle sizes due to water intake. Similarly, hygroscopic particle growth is evident for PRT following the rise in AI with WVC. This observation supports the evidence of the predominance of SS aerosols in CPT and sulphate-nitrate aerosol combination in the case of PRT, as depicted by the earlier figures (i.e., Figures 6a-6f).

3.3 Particle size distributions

The multiyear monthly average particle size distribution (PSD) for CPT in Figures 7a and 7b mainly displays bimodal characteristics that distinctly signify fine and coarse particles. Remarkably, the fine mode represents the region of radius (r) $< 0.4\mu$m and the coarse mode is marked by r) $< 0.4\mu$m. From the PSD variation in the figures, the coarse mode aerosol demonstrates a strong suggestion of predominance SS and possibly traces of MD. Several studies have shown that CPT is not prone to MD aerosol due to its general environmental characteristics, including not being within any desert regions proxies and possessing paved and tarred roads. However, the primary dust source is through occasional sedimentary weathering of rocks (Tesfaye et al., 2011; Yakubu & Chetty, 2020). The build-up of coarse mode volume concentration is observed in March and January, while a significant increase in fine mode particles notably occurred during July-September. These features are more apparent in the seasonal variation in Figure 7c, where distinct intensification of coarse mode particles is visible in summer, and peak concentration of fine mode aerosols is detectable in winter.

A substantial and distinct rise in the fine mode aerosol concentration (i.e., r $< 0.6\mu$m) is evident in February and September over PRT, thus demonstrating the predominance of fine particles as illustrated by the monthly average in Figures 7d and 7e. Additionally, several other peaks are observable in the region of r $> 0.6\mu$m, particularly for the months of May, June and September, as seen in the figures. These peaks represent the suspension of a significant amount of large-sized particles mainly due to the hygroscopic growth of hydrophilic aerosols (such as sulphate and nitrate) and emission from biomass burning activities (carbon soot), including from internal and external sources (i.e., considering the period of peak). This finding agrees well with the observation from several existing studies on the location (Adesina et al., 2016; Kumar et al., 2017; Yakubu & Chetty, 2022). Further to the monthly variation of PSD over PRT, Figure 7f displays the seasonal changes in the bimodal characteristics of the PSD. The highest concentrations of both coarse and fine mode aerosols are registered in spring, which depicts a scenario of mixed aerosol types linked to biomass burning and hydrophilic aerosols

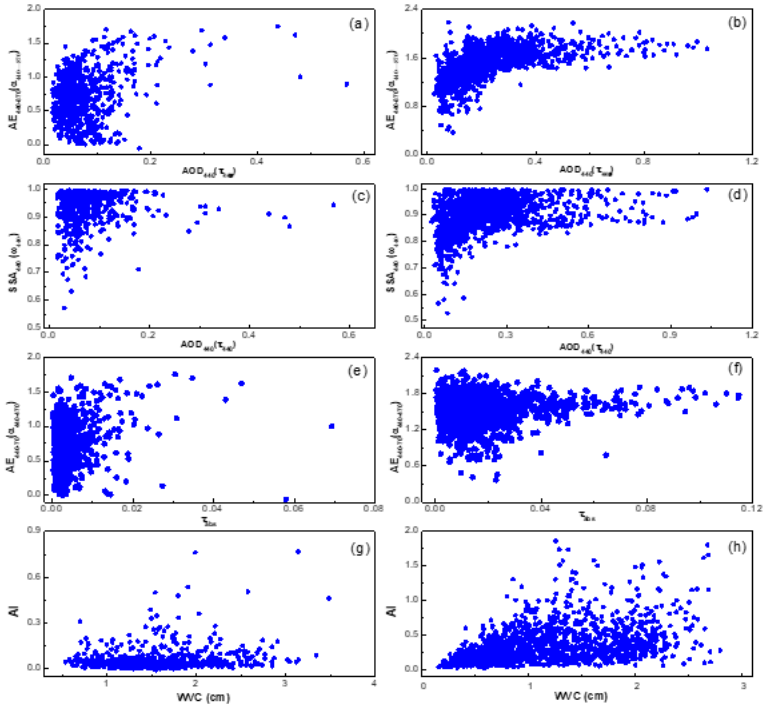

Figure 6. The plots of the relationships between AERONET, MISR and MODIS instrument measurement of the parameters AE vs AOD, SSA vs AOD, AE vs AOD_{abs} and AI vs WVC for CPT; (a), (c), (e) and (g), and PRT; (b), (d), (f) and (h)

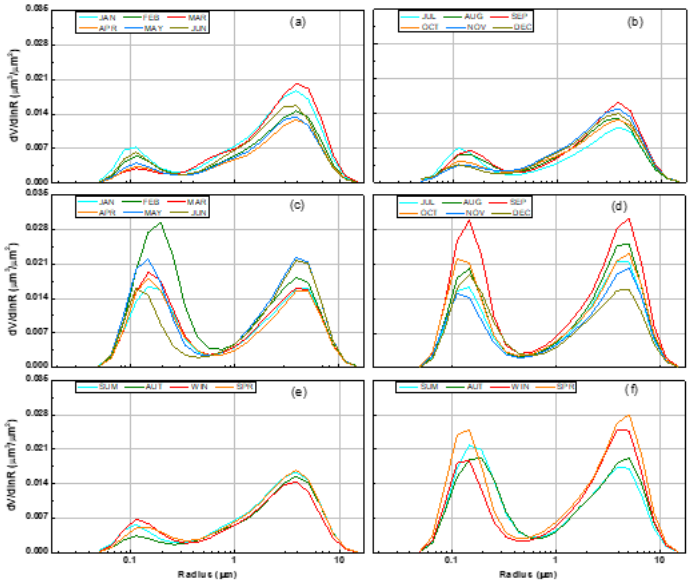

Figure 7. The illustration of monthly and seasonal average particle size distribution for CPT; (a), (C) and (e), and PRT; (b), (d) and (f))

3.4 Spectral Characteristics

The spectral behaviour of aerosol particles over the study locations is examined for wavelengths between 440-1020μm for AERONET, MISR and MODIS instruments. Figures 8a and 8b present the spectral characteristics of CPT and PRT, respectively. SSA in Figure 8a shows moderate spectral dependence such that ω is approximately steady between λ-values 440 and 680 nm, then slightly decreases with increasing wavelength at $\lambda > 680$ nm. This variation represents the mix of non-/absorbing aerosol typical for an urban-industrial setting that occasionally generates and receives an influx of absorbing particles like CPT. Meanwhile, the satellite observations of the spectral variation differ because both satellite instruments demonstrate increasing, then steady ω-values along with λ. The satellite observation from the MISR instrument follows the described pattern but approximately flattens as the wavelength changes. However, for MODIS, a strong spectral dependence of increasing ω with λ is visible for the few wavelengths range (i.e., 440-660nm) available for the instrument. Similarly, Figure 8b displays SSA exhibits moderate spectral dependence on wavelength, following ω sparingly decreasing with λ mainly at $\lambda > 800$ nm. The variation again indicates mixed-type aerosols of non-absorbing and absorbing properties which is consistent with the environmental situation of the PTR. MISR again exhibit closer similarity with the AERONET variation than MODIS, which is more divergent, just as experienced for CPT.

The variation of absorbing AOD for CPT illustrated in Figure 8c exhibits notable spectral dependency, mainly around $\lambda < 680$nm for the three instruments. An approximate steady value is noticeable for $\lambda > 680$nm. This variation shows the dominance of absorbing aerosol by fine particles and scattering aerosols by mainly coarse mode particles. The result from previous studies on this site has demonstrated similar variation (Yakubu & Chetty, 2020). Meanwhile, a strong spectral dependence is shown by AOD_{abs} over PRT in Figure 8d. AOD_{abs} decrease with increasing λ, and the pattern tends to be more evident at $\lambda < 680$nm. Like the pattern shown for CPT, smaller aerosol particles demonstrate higher absorption characteristics than larger ones. The AOD_{abs} spectral variation in PRT indicates a significant presence of absorbing fine mode aerosols such as BC and OC. Similar to the observation for CPT, the spectral characteristics of AOD_{abs} retrieved from MISR and MODIS instruments agree well with the AERONET measurement.

Apart from the spectral characteristics of ω and τ_{abs}, the refractive indices (i.e., the real and imaginary refractive index RI) also provide insights into the scattering and absorption properties of aerosol for possible identification of different aerosol types and size features. According to the trait exhibited by the real refractive index (RI_r) for CPT in Figure 8e, a significant change in the spectral behaviour of RI_r is observed such that it decreases with an increasing wavelength. This change is more apparent during the spring to autumn seasons. Since RI_r responds more to the scattering and particle size, the variation thus demonstrates the presence of a substantial amount of slightly large-sized absorbing aerosols (e.g., carbon soot). Further observation of the imaginary part of RI (RI_i) for CPT in Figure 8g, one can credibly notice an increase in absorption at $\lambda > 700$nm, which is consistent with the variation in Figure 8e. Thus, the average RI (RI_{av}) over CPT is 1.48 – i0.012, which is comparable to the RI of polluted urban marine environment (e.g., (Dubovik et al., 2002)).

In contrast, the RI_r for PRT in Figure 8f does not show strong spectral dependence as depicted by the RI_r for CPT, although the values (range 1.46-1.53) are higher than the observed values over CPT. These high values of RI_r are more evident for the winter and spring seasons associated with the intense emission of BB aerosol and particles from incomplete combustion of FF. Meanwhile, the lower values of RI_r for the other two seasons are liable to aerosol removal by increasing cloud developments and precipitation events. As for the RI_i in Figure 8h, the spectral dependence of RI with the wavelength is apparent at $\lambda < 650$nm and more associated with the winter and spring seasons. These

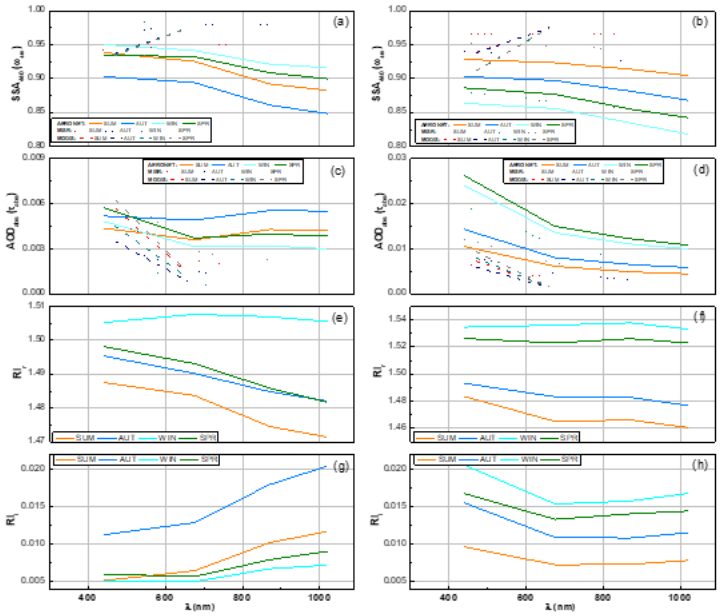

Figure 8. The graph showing the monthly and seasonal average spectral variation of SSA, AOD_{abs}, RI_r and RI_i for CTP (a, c, e and g) and PRT (b, d, f and h)

periods are primarily associated with increased fine mode absorbing aerosols mainly due to BB activities. Thus average RI_i for PRT decreases with λ, which with the variation of RI_r suggests the predominance of scattering aerosols. The mean RI over this site is 1.51 – i0.015, comparable to values recorded in BB polluted industrialised regions elsewhere (Dubovik et al., 2002).

3.5 Identification of the different aerosol types

After the aerosol properties examined in the previous sections, this section is intended to identify the prime aerosol types found in the locations under investigation. According to results from various existing studies (Boiyo et al., 2019; Giles et al., 2012; Smirnov et al., 2003), the behaviour of aerosol particles along the varying size range, absorption/scattering properties and the effect on light extinction constitute a vital and well-established method of inferring aerosol types. This is because different particle types differ in response to these attributes, although each feature cannot fully distinguish an aerosol type due to complex inter-similarities amongst particle types. Some studies have explored the methods of associating two or more properties to determine the different aerosol types in an environment (Boiyo et al., 2019; Kumar et al., 2017; Smirnov et al., 2003). However, these studies only consider particle size and aerosol loading or the size and absorbing/scattering characteristics. In this work, the particle effect on light extinction (AOD) and the absorption and scattering (ω and AOD_{abs}) are considered simultaneously to enhance the identification of the different aerosol types. The identification process mainly follows two

Table 2. Summary of the AOD, AOD_{abs} and SSA values associated with the different predominant aerosol types observed from the AERONET stations in (a) CPT and (b) PRT

(a)	Method I			Method II		
Type	τ range	τ_{abs} range	ω range	τ range	τ_{abs} range	ω range
SS	0.016 – 0.120	10^{-4} – 0.014	0.900 – 0.990	0.016 – 0.110	10^{-4} – 0.008	0.920 – 0.990
SO_4	0.140 – 0.570	10^{-4} – 0.024	0.920 – 0.994	0.080 – 0.234	$5x10^{-4}$ – 0.026	0.872 – 0.994
MD	0.016 – 0.140	0.002 – 0.021	0.800 – 0.900	0.016 – 0.171	0.001 – 0.031	0.827 – 0.930
OC	0.017 – 0.178	0.004 – 0.058	0.573 – 0.805	0.017 – 0.178	0.004 – 0.058	0.573 – 0.820
BC	0.150 – 0.480	0.016 – 0.069	0.840 – 0.913	0.279 – 0.480	0.019 – 0.069	0.850 – 0.937
(b)						
SS	0.032 – 0.090	$4x10^{-4}$ – 0.010	0.880 – 0.995	–	–	–
SO_4	0.080 – 0.379	$4x10^{-4}$ – 0.045	0.870 – 0.996	0.050 – 0.300	$4x10^{-4}$ – 0.049	0.810 – 0.996
MD	0.361 – 0.919	0.002 – 0.430	0.941 – 0.996	0.024 – 0.510	0.001 – 0.098	0.781 – 0.996
OC	0.037 – 0.370	0.005 – 0.078	0.527 – 0.870	0.026 – 0.250	0.002 – 0.065	0.527 – 0.980
BC	0.352 – 0.995	0.023 – 0.115	0.827 – 0.930	0.511 – 1.032	0.002 – 0.115	0.860 – 0.997

distinct procedures; (I) manual grouping of data points based on the scale of the three parameters under consideration and (II) application of clustering unsupervised machine learning (ML) algorithm using the three parameters as inputs.

Figure 9a shows the aerosol type classification based on AOD, ω and τ_{abs} for Cape Town using method (I). From the figure, five distinct clusters are identifiable. The cluster bounded by the red box represents the region of high scattering ($\omega > 0.89$), low aerosol loading ($\tau_{440} < 0.12$) and very low absorbing particles ($AOD_{abs} < 0.014$), which satisfy the features of SS aerosols and constitute the significant aerosol type over the site. The yellow box corresponding to high aerosol loading (AOD > 0.10), scattering ($\omega >$ 0.90) and low absorption ($AOD_{abs} < 0.02$) is linked to sulphate and nitrate aerosols. The orange box represents AOD < 0.02, 0.80 < ω < 0.90 and $AOD_{abs} < 0.02$ resembles more of MD. Also, the black box bounding particles with relatively low SSA ($\omega <$ 0.80), low to very high absorption, and AOD matches the carbonaceous soot and OC mix. At the same time, the cluster of AOD > 0.10, high absorbing and $\omega < 0.90$ (blue box) coincide with BC. Similarly, five distinct groups were detected using method (II) for CPT, as seen in Figure 9b. Generally, the clusters closely resembled those generated using method (I), although slight differences existed in boundaries defining each aerosol type. Table 2 fully describes detected boundaries defining the aerosol types obtained from both approaches.

Figure 10a illustrates the identification of the different dominating aerosol types over Pretoria based on the plot of AOD, SSA and AOD_{abs} using method (I). From the figure, the smallest cluster (red box) representing particles with high scattering and low absorption ($\omega > 0.9$, $AOD_{abs} < 0.02$ and AOD < 0.01) constitutes SS aerosols. The yellow box bounding high scattering aerosols with low absorption and AOD extending to high values matches sulphate and nitrate aerosols. Similarly, the region of high scattering (i.e.,$\omega > 0.92$), AOD ($\tau_{440} > 0.30$) and moderate to low absorbing feature (i.e., orange box) correspond to MD aerosols. Also, the cluster of particles having $\omega < 0.90$, low to moderate AOD_{abs}-values (i.e., 0.01 0.07), and AOD ranging from low to very high values bounded by the black box matches carbonaceous soot. Meanwhile, the segment of high absorbing, low scattering and high aerosol loading indicated by the blue box correspond to OC and BC mix.

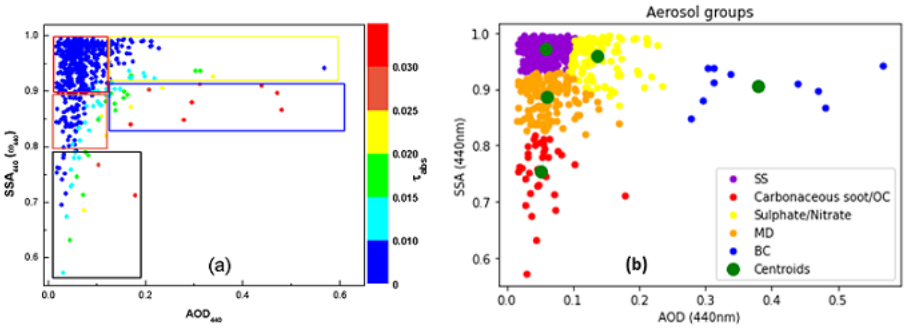

Figure 9. The cluster plot of different prime aerosol types based on the SSA, AOD and AOD_{abs} for CPT using procedure (a) I and (b) II

Unlike the output from method II for Cape Town that resulted in five distinct clusters similar to the pattern from its corresponding method I, four aerosol groups are detected for Pretoria using the machine learning approach. The identified clusters from method I substantially differ from those displayed by method II for the location, particularly around the region of AOD > 0.4 and high AOD_{abs}-values, as seen in Figure 10b. A summary of the identified clusters of crucial aerosol types is thus presented in Table 2. Hence from the identification process, sulphate and nitrate aerosols are the predominant aerosol types in the region which is consistent with the urban-industrialised characteristic of the location. Likewise significant is the identification of a substantial amount of carbonaceous aerosols (soot, OC and BC) being in suspension over the region and earlier suggested to result from local and external activities of BB. The results from aerosol observations and identifications for the two locations closely agree with several studies conducted over these sites and elsewhere globally (Boiyo et al., 2019; Kumar et al., 2017; Smirnov et al., 2003; Yakubu & Chetty, 2020).

3.6 Radiative forcing (RF)

A crucial impact of aerosol on the earth associated with huge uncertainties is the radiative forcing (RF) effect. The RF, which constitutes the primary factor that influences the global average temperature and is a critical climate driver, is a function of the amount of incoming shortwave (SWR) solar radiation and outgoing longwave (LWR) terrestrial radiation (IPCC, 2007, 2013). The effective RF mainly results in a net cooling effect when incoming SWR is lesser than outgoing LWR, a condition typical of predominated scattering aerosols. In contrast, a net warming effect occurs when SWR $>$ LWR, is mainly enhanced by absorbing particles (Kumar et al., 2017; Lohmann & Feichter, 2005).

Therefore, Figure 11 displays the multiyear average monthly RF at the bottom of the atmosphere (BOA), the top of the atmosphere (TOA) and ARF for Cape Town and Pretoria as observed from the AERONET instrument at each site. In Figure 11a, the

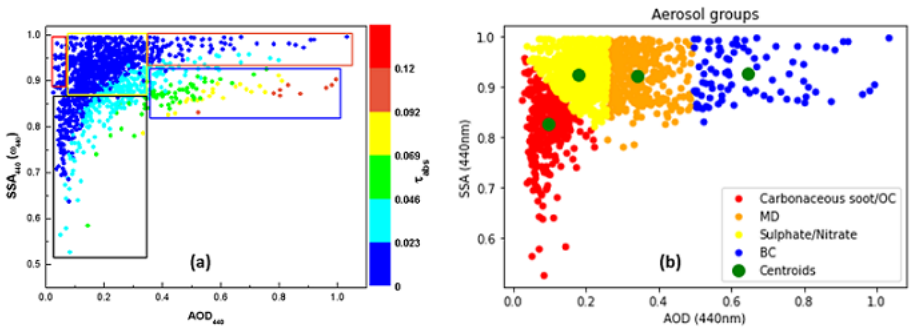

Figure 10. The cluster plot of different prime aerosol types based on the SSA, AOD and AOD_{abs} for PRT using procedure (a) I and (b) II

RF_{BOA} for CPT generally demonstrated a warming effect over the region with an overall average of 11.31 $\pm$2.01Wm^{-2}. The maximum monthly average of 14.50Wm^{-2} in September corresponds to the high aerosol loading period associated with the influx of aged smoke from BB activities outside the region. In comparison, the minimum 8.35Wm^{-2} in May coincides with the period of low aerosol loading. Similarly, for Pretoria in Figure 11b, a positive RF of a monthly average of 26.01Wm^{-2} is observed at the BOA leading to a warming effect. The maximum RF at BOA (45.55Wm^{-2}) recorded in September is linked to the activities of BB in the region and from boundary communities. Also, the peak coincides with the maximum over CPT, emphasising the drift of BB aerosol from the dominating sources in the north to the southern part of Southern Africa. Meanwhile, the minimum monthly value (18.97 Wm^{-2}) occurs in January and coincide with the period dominated by internally generated aerosols.

The RF at TOA depicts a negative forcing over CPT in contrast to the pattern shown by RF at BOA (see Figure 11a). The average monthly RF at TOA for the multiyear statistics is -5.34 $\pm$1.04Wm^{-2}, representing a cooling effect. From the chat, the maximum cooling effect (-6.49Wm^{-2}) occurs in September, while the minimum (-3.36Wm^{-2}) is recorded in March. For the PRT station (see Figure 11b), a similitude variation, as earlier seen in the case of CPT, is evident. A cooling effect with a multiyear monthly average value of -10.30 $\pm$1.91Wm^{-2} is observed at TOA over PRT. Meanwhile, the maximum negative RF at TOA is -14.20Wm^{-2} in February, and the minimum cooling effect is -7.56Wm^{-2}, which occurs in June. Therefore, the variation of RF at TOA demonstrated by both locations depicts the consequences of predominance scattering initiated by a differing factor such that coarse aerosol (SS) is linked to CPT, and fine particles (sulphate and nitrate aerosol) are associated with PRT.

According to the expression in equation (1), the effective RF (i.e., ARF) for the study locations, as shown in Figure 11 (a and b), apparently display net cooling effects (negative RF) over the two sites. Over CPT, an average net cooling effect of value -16.65

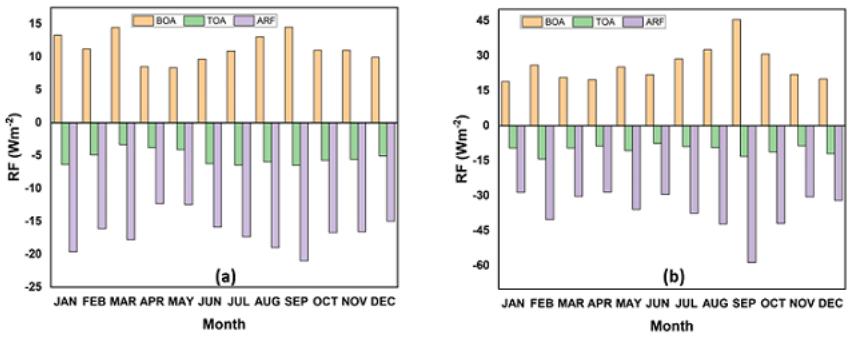

Figure 11. The graph of RF at BOA, TOA and average over CPT (a) and Pretoria (b)

$\pm 2.40 \mathrm{Wm}^{-2}$ is estimated over the location during the study period. The maximum cooling effect ($-20.99 \mathrm{Wm}^{-2}$) is attained during September, and the minimum ($-12.32 \mathrm{Wm}^{-2}$) is reached in April. Also, a net cooling effect averaged at -36.31 $\pm$8.36 Wm^{-2} in PRT during the study period. The monthly mean cooling effect at maximum ($-58.68 \mathrm{Wm}^{-2}$) occurs in September, coinciding with the month of higher aerosol loading. And as expected, the minimum cooling effect ($-28.55 \mathrm{Wm}^{-2}$) occurred during January, which is identified for low AOD. One can see that the net RF over the two locations result in a practical cooling effect. The magnitude of cooling is higher over PRT than CPT and significantly depends on the aerosol loading and the predominance of aerosol types suspended over the regions.

4 Conclusion

The optical properties and the consequential radiative effect of aerosol are investigated in Cape Town (CPT) and Pretoria (PRT), two renowned metropolitans with distinct background aerosol types and commonly influenced by biomass burning (BB) activities from the northern part of South Africa. Apart from the background aerosol, they differ in meteorological and climate circumstances due to geographical stance and internal activities. Thus, the followings are deduced from the observations.

Cape Town is mainly characterised by low aerosol loading predominated by coarse particles identified as sea salt (SS). In contrast, Pretoria is found to experience high aerosol loading, largely fine mode particles ailing from different combustion activities (i.e., BB and fossil fuel combustion). Furthermore, the aerosol loading over the two metropolitans is frequently influenced by BB activities emitted north of South Africa, including PRT during the pre-farming season in September, which alters aerosols spectral and radiative properties over the locations.

Aerosol suspension over CPT and PRT mainly demonstrated strong scattering characteristics and low absorption properties. While CPTs high scattering and low absorp-

tion characteristics are linked to coarse mode aerosols of marine origin (SS aerosols), suspension over PRT is more of fine mode particles ascribed to sulphate and nitrate aerosols. Further, the aerosol absorption feature increases in both locations during the period identified for the predominance of BB activities, with the prevalence more obvious for PRT.

The columnal precipitable water increases sharply over the two locations during summer, representing more than 65% compared to the values during the other sea seasons. Also, the average value for WVC is slightly higher in CPT than in PRT. Cape Towns nearness to the ocean is accountable for its higher values than PRT.

Validation of satellite instrument measurements of aerosol parameters against the AERONET datasets shows considerable agreement. However, some parameters such as AE, AOD_{abs} and SSA demonstrated poor agreement and large uncertainty regarding the ground instrument for specific locations and different platforms. On a general note, MODIS outperformed MISR in retrievals of most parameters and provided an exceptional dataset of atmospheric vapour measurement (i.e., for WVC, $R > 0.95$), which is unavailable for MISR. Considering the two locations, the satellite retrieval possesses better accuracy in PRT (mainly land surface) than for CPT (water environment).

Analysis based on the optical and spectral characteristics of the parameters under consideration (SSA, AOD_{abs}, RI_r and RI_i), the ranking of prominence aerosol types suspended over CPT follows the hierarchy MD < OC < BC < sulphate/nitrate < SS. Similarly, for PRT, the order of prominence follows SS < MD < OC < BC < sulphate/nitrate aerosols. Also, machine learning techniques demonstrate the capability to classify and identify different aerosol types based on their optical features.

The effective radiative forcing over the two locations is negative, resulting in net cooling effects and primarily influenced by different aerosol types in each case. Over CPT, the predominance of SS aerosols is observed to be responsible for this condition. In contrast, the prevalence of sulphate/nitrate aerosols is identified as the culprit for the net cooling effect over PRT.

Open Research Section

The datasets used in presenting the result in this work are obtainable from: https://www.aeronet.gsfc.nasa.g
bin for AERONET, https://www.asdc.larc.nasa.gov/data/MISR for MISR, https://www.ladsweb.modaps.eosdis.n
for MODIS and https://www.lpdaac.usgs.gov/products/mcd43a1v061 for MODIS albedo products only.

Acknowledgments

The authors wish to acknowledge the principal investigators of the AERONET sites in Pretoria and Simonstown for making the data available. The are also thankful to the MISR and MODIS team and their respective data distribution archive centre for the efforts toward making these scientific data available.

References

Abdou, W. A., Diner, D. J., Martonchik, J. V., Bruegge, C. J., Kahn, R. A., Gaitley, B. J., ... Holben, B. (2005). Comparison of coincident multiangle imaging spectroradiometer and moderate resolution imaging spectroradiometer aerosol optical depths over land and ocean scenes containing aerosol robotic network sites [Journal Article]. *Journal of Geophysical Research*, *110*(D10). doi: 10.1029/2004jd004693

Ackerman, A. S., Toon, O. B., Stevens, D. E., Heymsfield, A. J., Ramanathan, V., & Welton, E. J. (2000). Reduction of tropical cloudiness by soot [Jour-

nal Article]. *Science*, *288*(5468), 1042-1047. Retrieved from https://science.sciencemag.org/content/sci/288/5468/1042.full.pdf doi: 10.1126/science.288.5468.1042

Adesina, A. J., Kumar, K. R., & Sivakumar, V. (2016). Aerosol-cloud-precipitation interactions over major cities in south africa: Impact on regional environment and climate change [Journal Article]. *Aerosol and Air Quality Research*, *16*(1), 195-211. Retrieved from https://doi.org/10.4209/aaqr.2015.03.0185 doi: 10.4209/aaqr.2015.03.0185

Boiyo, R., Kumar, K. R., Zhao, T., & Guo, J. (2019). A 10-year record of aerosol optical properties and radiative forcing over three environmentally distinct aeronet sites in kenya, east africa [Journal Article]. *Journal of Geophysical Research: Atmospheres*, *124*(3), 1596-1617. doi: 10.1029/2018jd029461

Boucher, O. (2015). *Atmospheric aerosols: Properties and climate impacts* (1st ed.) [Book]. Netherlands: Springer. Retrieved from https://www.springer.com/gp/book/9789401796484 doi: 10.1007/978-94-017-9649-1

Charlson, R. J., Schwartz, S. E., Hales, J. M., Cess, R. D., Coakley, J., J. A., Hansen, J. E., & Hofmann, D. J. (1992). Climate forcing by anthropogenic aerosols [Journal Article]. *Science*, *255*(5043), 423-30. Retrieved from https://www.ncbi.nlm.nih.gov/pubmed/17842894 doi: 10.1126/science.255.5043.423

Christensen, M. W., & Stephens, G. L. (2012). Microphysical and macrophysical responses of marine stratocumulus polluted by underlying ships: 2. impacts of haze on precipitating clouds [Journal Article]. *Journal of Geophysical Research-Atmospheres*, *117*(D11203). Retrieved from <GotoISI>://WOS:000304766700003 doi: ArtnD1120310.1029/2011jd017125

de Leeuw, G., Andreas, E. L., Anguelova, M. D., Fairall, C. W., Lewis, E. R., O'Dowd, C., ... Schwartz, S. E. (2011). Production flux of sea spray aerosol [Journal Article]. *Reviews of Geophysics*, *49*(2). doi: 10.1029/2010rg000349

de Meij, A., & Lelieveld, J. (2011). Evaluating aerosol optical properties observed by ground-based and satellite remote sensing over the mediterranean and the middle east in 2006 [Journal Article]. *Atmospheric Research*, *99*(3-4), 415-433. doi: 10.1016/j.atmosres.2010.11.005

Diner, D. J., Beckert, J. C., Reilly, T. H., Bruegge, C. J., Conel, J. E., Kahn, R. A., ... Verstraete, M. M. (1998). Multiangle image spectroradiometer (misr) instrument description and experiment overview [Journal Article]. *IEEE T. Geosci. Remote*, *36*, 10721087. doi: https://doi.org/10.1109/36.700992

Drury, E., Jacob, D. J., Wang, J., Spurr, R. J. D., & Chance, K. (2008). Improved algorithm for modis satellite retrievals of aerosol optical depths over western north america [Journal Article]. *Journal of Geophysical Research: Atmospheres*, *113*(D16). Retrieved from https://doi.org/10.1029/2007JD009573 doi: 10.1029/2007JD009573

Dubovik, O., Holben, B., Eck, T. F., Smirnov, A., Kaufman, Y. J., King, M. D., ... Slutsker, I. (2002). Variability of absorption and optical properties of key aerosol types observed in worldwide locations [Journal Article]. *Journal of the Atmospheric Sciences*, *59*(3), 590-608. Retrieved from https://journals.ametsoc.org/view/journals/atsc/59/3/1520-0469_2002_059_0590_voaaop_2.0.co_2.xml doi: https://doi.org/10.1175/1520-0469(2002)059⟨0590:VOAAOP⟩2.0.CO;2

Dubovik, O., & King, M. D. (2000). A flexible inversion algorithm for retrieval of aerosol optical properties from sun and sky radiance measurements [Journal Article]. *Journal of Geophysical Research: Atmospheres*, *105*(D16), 20673-20696. Retrieved from https://agupubs.onlinelibrary.wiley.com/doi/abs/10.1029/2000JD900282 doi: 10.1029/2000jd900282

Eck, T. F., Holben, B. N., Reid, J. S., Mukelabai, M. M., Piketh, S. J., Torres, O., ... Slutsker, I. (2013). A seasonal trend of single scattering albedo in south-

ern african biomass-burning particles: Implications for satellite products and estimates of emissions for the world's largest biomass-burning source [Journal Article]. *Journal of Geophysical Research: Atmospheres*, *118*(12), 6414-6432. Retrieved from https://agupubs.onlinelibrary.wiley.com/doi/abs/10.1002/jgrd.50500 doi: 10.1002/jgrd.50500

Falaiye, O., Yakubu, A., Aweda, F., & Abimbola, O. (2013). Mineralogical characteristics of harmattan dust in ilorin, sub-sahara africa [Journal Article]. *Ife Journal of Science*, *15*(1), 175-181. Retrieved from https://www.ajol.info/index.php/ijs/article/view/131411/121007

Fan, J., Wang, Y., Rosenfeld, D., & Liu, X. (2016). Review of aerosolcloud interactions: Mechanisms, significance, and challenges [Journal Article]. *Journal of the Atmospheric Sciences*, *73*(11), 4221-4252. doi: 10.1175/jas-d-16-0037.1

Formenti, P., Winkler, H., Fourie, P., Piketh, S., Makgopa, B., Helas, G., & Andreae, M. O. (2002). Aerosol optical depth over a remote semi-arid region of south africa from spectral measurements of the daytime solar extinction and the nighttime stellar extinction [Journal Article]. *Atmospheric Research*, *62*(1-2), 11-32. Retrieved from www.elsevier.com/locate/atmos doi: 10.1016/S0169-8095(02)00021-2

Gettelman, A., & Sherwood, S. C. (2016). Processes responsible for cloud feedback [Journal Article]. *Current Climate Change Reports*, *2*(4), 179-189. Retrieved from https://doi.org/10.1007/s40641-016-0052-8 doi: 10.1007/s40641-016-0052-8

Giles, D. M., Holben, B. N., Eck, T. F., Sinyuk, A., Smirnov, A., Slutsker, I., ... Schafer, J. S. (2012). An analysis of aeronet aerosol absorption properties and classifications representative of aerosol source regions [Journal Article]. *Journal of Geophysical Research: Atmospheres*, *117*(D17). Retrieved from https://agupubs.onlinelibrary.wiley.com/doi/abs/10.1029/2012JD018127 doi: 10.1029/2012jd018127

Hansen, J., Sato, M., & Ruedy, R. (1997). Radiative forcing and climate response [Journal Article]. *Journal of Geophysical Research: Atmospheres*, *102*(D6), 6831-6864. Retrieved from https://agupubs.onlinelibrary.wiley.com/doi/abs/10.1029/96JD03436 doi: 10.1029/96jd03436

Haywood, J., & Boucher, O. (2000). Estimates of the direct and indirect radiative forcing due to tropospheric aerosols: A review [Journal Article]. *Reviews of Geophysics*, *38*(4), 513-543. Retrieved from <GotoISI>://WOS:000165171200004 doi: Doi10.1029/1999rg000078

Hersey, S. P., Garland, R. M., Crosbie, E., Shingler, T., Sorooshian, A., Piketh, S., & Burger, R. (2015). An overview of regional and local characteristics of aerosols in south africa using satellite, ground, and modeling data [Journal Article]. *Atmospheric chemistry and physics*, *15*, 4259-4278. Retrieved from https://www.ncbi.nlm.nih.gov/pubmed/26312061https://www.ncbi.nlm.nih.gov/pmc/articles/PMC4547400/ doi: 10.5194/acp-15-4259-2015

Hodnebrog, ., Myhre, G., Forster, P. M., Sillmann, J., & Samset, B. H. (2016). Local biomass burning is a dominant cause of the observed precipitation reduction in southern africa [Journal Article]. *Nature Communications*, *7*(1), 11236. Retrieved from https://doi.org/10.1038/ncomms11236 doi: 10.1038/ncomms11236

Holben, B. N., Eck, T. F., Slutsker, I., Tanr, D., Buis, J. P., Setzer, A., ... Smirnov, A. (1998). Aeroneta federated instrument network and data archive for aerosol characterization [Journal Article]. *Remote Sensing of Environment*, *66*(1), 1-16. Retrieved from http://www.sciencedirect.com/science/article/pii/S0034425798000315 doi: https://doi.org/10.1016/S0034-4257(98)00031-5

Ichoku, C., Remer, L. A., Kaufman, Y. J., Levy, R. C., Chu, D., Tanr, D., & Holben, B. N. (2003). Modis observation of aerosols and estimation of aerosol radiative forcing over southern africa during safari 2000 [Journal Article]. *J.*

Geophys. Res., *108*(D13). doi: 10:1029/2002JD002366

IPCC. (2007, 2007). *The physical science basis. contribution of working group i to the forth assessment report of the intergovernmental panel on climate change* (Report). Cambridge University Press.

IPCC. (2013). *Climate change 2013: The physical science basis. contribution of working group i to the fifth assessment report of the intergovernmental panel on climate change* [Book]. Cambridge, United Kingdom and New York, NY, USA: Cambridge University Press. Retrieved from www.climatechange2013.org doi: 10.1017/CBO9781107415324

Jacobson, M. Z. (2001). Global direct radiative forcing due to multicomponent anthropogenic and natural aerosols [Journal Article]. *Journal of Geophysical Research: Atmospheres*, *106*(D2), 1551-1568. doi: 10.1029/2000jd900514

Kahn, R. A., Gaitley, B. J., Garay, M. J., Diner, D. J., Eck, T. F., Smirnov, A., & Holben, B. N. (2010). Multiangle imaging spectroradiometer global aerosol product assessment by comparison with the aerosol robotic network [Journal Article]. *Journal of Geophysical Research*, *115*(D23). doi: 10.1029/2010jd014601

Kaufman, Y. J., Holben, B. N., Tanr, D., Slutsker, I., Smirnov, A., & Eck, T. F. (2000). Will aerosol measurements from terra and aqua polar orbiting satellites represent the daily aerosol abundance and properties? [Journal Article]. *Geophysical Research Letters*, *27*(23), 3861-3864. Retrieved from https://agupubs.onlinelibrary.wiley.com/doi/abs/10.1029/2000GL011968 doi: 10.1029/2000gl011968

Kaufman, Y. J., Tanr, D., Gordon, H. R., Nakajima, T., Lenoble, J., Frouin, R., ... Teillet, P. M. (1997). Passive remote sensing of tropospheric aerosol and atmospheric correction for the aerosol effect [Journal Article]. *Journal of Geophysical Research: Atmospheres*, *102*(D14), 16815-16830. Retrieved from https://agupubs.onlinelibrary.wiley.com/doi/abs/10.1029/97JD01496 doi: 10.1029/97jd01496

Kumar, K. R., Kang, N., Sivakumar, V., & Griffith, D. (2017). Temporal characteristics of columnar aerosol optical properties and radiative forcing (20112015) measured at aeronets pretoria-csir-dpss site in south africa [Journal Article]. *Atmospheric Environment*, *165*, 274-289. doi: DOI10.1016/j.atmosenv.2017.06.048

Lohmann, U., & Feichter, J. (2005). Global indirect aerosol effects: a review [Journal Article]. *Atmospheric Chemistry and Physics*, *5*, 715-737. Retrieved from <GotoISI>://WOS:000227375000002 doi: DOI10.5194/acp-5-715-2005

Lora-Salazar, S. M., Holmes, H. A., Patrick Arnott, W., Barnard, J. C., & Moosmller, H. (2016). Evaluation of modis columnar aerosol retrievals using aeronet in semi-arid nevada and california, u.s.a., during the summer of 2012 [Journal Article]. *Atmospheric Environment*, *144*, 345-360. Retrieved from http://www.sciencedirect.com/science/article/pii/S1352231016306690 doi: https://doi.org/10.1016/j.atmosenv.2016.08.070

McBride, C. M., Kruger, A. C., & Dyson, L. (2022). Changes in extreme daily rainfall characteristics in south africa: 19212020 [Journal Article]. *Weather and Climate Extremes*, *38*, 100517. Retrieved from https://www.sciencedirect.com/science/article/pii/S2212094722000962 doi: https://doi.org/10.1016/j.wace.2022.100517

Pope, C. A., Burnett, R. T., Thun, M. J., Calle, E. E., Krewski, D., Ito, K., & Thurston, G. D. (2002). Lung cancer, cardiopulmonary mortality, and long-term exposure to fine particulate air pollution [Journal Article]. *JAMA*, *287*(9), 1132-1141. Retrieved from https://doi.org/10.1001/jama.287.9.1132 doi: 10.1001/jama.287.9.1132

Putaud, J. (2010). European aerosol phenomenology-3: Physical and chemical characteristics of particulate matter from 60 rural, urban, and kerbside sites across

europe [Journal Article]. *Atmospheric Environment*, *44*, 13.

Queface, A. J., Piketh, S. J., Eck, T. F., Tsay, S. C., & Mavume, A. F. (2011). Climatology of aerosol optical properties in southern africa [Journal Article]. *Atmospheric Environment*, *45*(17), 2910-2921. Retrieved from <GotoISI>://WOS:000291079300012 doi: 10.1016/j.atmosenv.2011.01.056

Rosenfeld, D. (1999). Trmm observed first direct evidence of smoke from forest fires inhibiting rainfall [Journal Article]. *Geophysical Research Letters*, *26*(20), 3105-3108. Retrieved from https://doi.org/10.1029/1999GL006066 doi: 10.1029/1999GL006066

Rosenfeld, D., Andreae, M. O., Asmi, A., Chin, M., de Leeuw, G., Donovan, D. P., ... Quaas, J. (2014). Global observations of aerosol-cloud-precipitation-climate interactions [Journal Article]. *Reviews of Geophysics*, *52*(4), 750-808. doi: 10.1002/2013rg000441

Sayer, A. M., Hsu, N. C., Eck, T. F., Smirnov, A., & Holben, B. N. (2014). Aeronet-based models of smoke-dominated aerosol near source regions and transported over oceans, and implications for satellite retrievals of aerosol optical depth [Journal Article]. *Atmospheric Chemistry and Physics*, *14*(20), 11493-11523. Retrieved from https://www.atmos-chem-phys.net/14/11493/2014/ doi: 10.5194/acp-14-11493-2014

Schuster, G. L., Vaughan, M., MacDonnell, D., Su, W., Winker, D., Dubovik, O., ... Trepte, C. (2012). Comparison of calipso aerosol optical depth retrievals to aeronet measurements, and a climatology for the lidar ratio of dust [Journal Article]. *Atmospheric Chemistry and Physics*, *12*(16), 7431-7452. Retrieved from https://www.atmos-chem-phys.net/12/7431/2012/ doi: 10.5194/acp-12-7431-2012

Schwartz, S. E., Harshvardhan, & Benkovitz, C. M. (2002). Influence of anthropogenic aerosol on cloud optical depth and albedo shown by satellite measurements and chemical transport modeling [Journal Article]. *Proc Natl Acad Sci U S A*, *99*(4), 1784-9. Retrieved from https://www.ncbi.nlm.nih.gov/pubmed/11854481 doi: 10.1073/pnas.261712099

Seinfeld, J. H., Bretherton, C., Carslaw, K. S., Coe, H., DeMott, P. J., Dunlea, E. J., ... Wood, R. (2016). Improving our fundamental understanding of the role of aerosol-cloud interactions in the climate system [Journal Article]. *Proc Natl Acad Sci U S A*, *113*(21), 5781-5790. Retrieved from https://www.ncbi.nlm.nih.gov/pubmed/27222566 doi: 10.1073/pnas.1514043113

Sen Roy, S., & Rouault, M. (2013). Spatial patterns of seasonal scale trends in extreme hourly precipitation in south africa [Journal Article]. *Applied Geography*, *39*, 151-157. Retrieved from https://www.sciencedirect.com/science/article/pii/S014362281200166X doi: https://doi.org/10.1016/j.apgeog.2012.11.022

Sherman, J. P., Gupta, P., Levy, R. C., & Sherman, P. J. (2016). An evaluation of modis-retrieved aerosol optical depth over a mountainous aeronet site in the southeastern us [Journal Article]. *Aerosol and Air Quality Research*, *16*(12), 3243-3255. Retrieved from https://doi.org/10.4209/aaqr.2015.09.0568 doi: 10.4209/aaqr.2015.09.0568

Sioris, C. E., Zou, J., McElroy, C. T., Boone, C. D., Sheese, P. E., & Bernath, P. F. (2016). Water vapour variability in the high-latitude upper troposphere part 2: Impact of volcanic eruptions [Journal Article]. *Atmospheric Chemistry and Physics*, *16*(4), 2207-2016. Retrieved from https://www.atmos-chem-phys.net/16/2207/2016/ doi: 10.5194/acp-16-2207-2016

Smirnov, A., Holben, B. N., Dubovik, O., Frouin, R., Eck, T. F., & Slutsker, I. (2003). Maritime component in aerosol optical models derived from aerosol robotic network data [Journal Article]. *Journal of Geophysical Research-Atmospheres*, *108*(D1). Retrieved from <GotoISI>://WOS:000181576800014 doi: Artn403310.1029/2002jd002701

Smirnov, A., Holben, B. N., Dubovik, O., O'Neill, N. T., Eck, T. F., Westphal, D. L., ... Slutsker, I. (2002). Atmospheric aerosol optical properties in the persian gulf [Journal Article]. *Journal of the Atmospheric Sciences*, *59*(3), 620-634. Retrieved from https://doi.org/10.1175/1520-0469(2002)059<0620:AAOPIT>2.0.CO;2 doi: 10.1175/1520-0469(2002)059⟨0620:AAOPIT⟩2.0.CO;2

Tesfaye, M., Sivakumar, V., Botai, J., & Mengistu Tsidu, G. (2011). Aerosol climatology over south africa based on 10 years of multiangle imaging spectroradiometer (misr) data [Journal Article]. *Journal of Geophysical Research: Atmospheres*, *116*(D20). Retrieved from https://agupubs.onlinelibrary.wiley.com/doi/abs/10.1029/2011JD016023 doi: 10.1029/2011jd016023

Twomey, S. (1977). Influence of pollution on shortwave albedo of clouds [Journal Article]. *Journal of the Atmospheric Sciences*, *34*(7), 1149-1152. Retrieved from <GotoISI>://WOS:A1977DP78800020 doi: Doi10.1175/1520-0469(1977)034⟨1149:Tiopot⟩2.0.Co;2

Wang, D., Jiang, B., Li, F., & Lin, W. (2018). Investigation of the air pollution event in beijing-tianjin-hebei region in december 2016 using wrf-chem [Journal Article]. *Advances in Meteorology*, *2018*, 1-12.

Wang, D., Liang, S., He, T., Yu, Y., Schaaf, C., & Wang, Z. (2015). Estimating daily mean land surface albedo from modis data [Journal Article]. *J. Geophys. Res.*, *120*(10), 4825-4841. doi: 10.1002/2015JD023178

Yakubu, A. T., & Chetty, N. (2020). Optical properties of atmospheric aerosol over cape town, western cape of south africa: Role of biomass burning [Journal Article]. *Atmsfera*, *34*(4), 395416. doi: 10.20937/52811

Yakubu, A. T., & Chetty, N. (2022). A decadal assessment of the climatology of aerosol and cloud properties over south africa [Journal Article]. *Atmos. Chem. Phys.*, *22*(17), 11065-11087. Retrieved from https://acp.copernicus.org/articles/22/11065/2022/ doi: 10.5194/acp-22-11065-2022

Yun, L., Yuan, W., Bowen, P., Jiaxi, H., Song, G., Misti, L., ... Renyi, Z. (2022). Formation , radiative forcing, and climatic effects of severe regional haze [Journal Article]. *Atmos. Chem. Phys*, *22*, 4951-4967. doi: 10.5195/acp-22-4951-2022

Atmospheric aerosol optical properties and radiative forcing over two metros in South Africa

Abdulaziz T. Yakubu[1], and Naven Chetty[1]

[1]Discipline of Physics, School of Chemistry and Physics, University of KwaZulu-Natal, Pietermaritzburg, 3209, South Africa

Key Points:

- The radiative forcing over South Africa is a net negative effect mainly associated with sea salt aerosol in the south and sulphate/nitrate aerosol in the north.
- A seasonal drift in absorbing aerosol concentration is observed from north to south and often influences aerosol suspension's optical and spectral characteristics over the region leading to decreasing cooling effect.
- The satellite retrieval over South Africa demonstrated significant agreement with AERONET measurements and mainly over the land than the water.

Corresponding author: Naven Chetty, `chettyn3@ukzn.ac.za`

Abstract

Aerosol Robotic Network (AERONET) measurement data is used in the validation of two prominent satellite aerosol property retrieval, Multiangle Imaging Spectroradiometer (MISR) and Moderate Resolution Imaging Spectroradiometer (MODIS), then applied to examine the properties of aerosols and the direct influence on radiative forcing (RF) over two metropolitan cities, Cape Town (CPT) and Pretoria (PRT) in South Africa. The synoptic characteristics of aerosols over CPT for 2015-2019 indicate a general low aerosol optical depth (AOD) of an average of 0.08 $\pm$ 0.014 and are prevalently sea salt (SS) aerosols. In contrast, a high AOD value with an average of 0.23 $\pm$ 0.050 was observed over PRT between 2011-2019 and predominated by sulphate/nitrate aerosols. These two dominant aerosol types are found to be the primary motivator of the net cooling effect of RF due to aerosol in each location. While the average RF over CPT is -16.79 $\pm$ 5.61 during the study period, the value over PRT is estimated to be more than two times (-36.55 $\pm$ 10.54) of the former. The validation of MISR and MODIS satellite aerosol properties retrieval for the region demonstrated better accuracy over the land than in the maritime environment. Meanwhile, MODIS underestimated AOD by $\approx$ 32% but generally reported better precision across the board than the MISR instrument. Further investigation into the seasonal variation of aerosols over the two locations identified seasonality changes in the characteristics of aerosols mainly influenced by the transport of high-absorbing biomass-burning aerosols.

Plain Language Summary

Air pollutants from human and natural resources often modify the amount of energy reaching the earths surface from the sun. Over South Africa, an enhanced cooling effect is often experienced due to the predominantly scattering characteristics of suspended particles. However, occasionally induced absorbing pollutants from the northern part of the region diffused southward and changed the atmospheric characteristics of the area. The extent of influence over parts of the region significantly depends on the proximity to the prime aerosol sources.

1 Introduction

Atmospheric aerosols are known to influence global weather and climate conditions. However, the extent of this influence solely and relative to other components that impact observable changes in the weather and climate system forms a significant source of ambiguity (Boucher, 2015; IPCC, 2013). Aerosol particles significantly interact with incoming solar radiation directly through scattering and absorption and indirectly by modifying the clouds microphysical properties (Haywood & Boucher, 2000) while serving as cloud condensation and ice nuclei (CCN and IN) during cloud formation (Ackerman et al., 2000; Twomey, 1977). Also, they interact with terrestrial (longwave) radiation via absorption and re-emission to alter the amount of outgoing electromagnetic radiation (Hansen et al., 1997). The interaction of these particles with solar as the primary energy source and terrestrial radiations results in the earths energy budget perturbation, which often drives the changes in weather and climate conditions (Hansen et al., 1997; Haywood & Boucher, 2000). More so, aerosols influence differing atmospheric and environmental challenges ranging from poor air quality, health problems, low visibility, and a dusty environment (Falaiye et al., 2013; Pope et al., 2002; Putaud, 2010) which are detrimental to human survival and general well-being. In contrast, aerosols are vital components of cloud formation and rainfall and sometimes serve as an essential source of soil nutrients favourable to humans (Falaiye et al., 2013; Fan et al., 2016). Therefore, regular qualitative and quantitative assessments are crucial for properly managing its consequences regarding their impacts on the earths energy budget and humans.

Aerosols are emitted from different sources, vary in types and properties, and the distribution is susceptible to spatio-temporal changes (Yakubu & Chetty, 2020). Furthermore, based on the listed characteristics, aerosol particles influence the earth and its atmosphere to varying degrees on a regional and global scale (IPCC, 2013). However, due to the poor understanding of how different aerosol characteristics translate to differing atmospheric and climate changes, their impacts are associated with significant uncertainty (IPCC, 2013; Jacobson, 2001). Similarly, the knowledge and uncertainty gaps in characterising and quantifying aerosol effects result in their underrepresentation in the cloud and the general circulation model (GCM) (Gettelman & Sherwood, 2016; Seinfeld et al., 2016). Therefore, proper quantification of the variation and roles of different aerosol types become critical in characterising their corresponding effects efficiently.

Over the years, various approaches have been employed to measure and determine aerosol characteristics, including in-situ measurement, ground and satellite remote sensing, and modelling (de Meij & Lelieveld, 2011; Drury et al., 2008; Dubovik & King, 2000). Each process has distinct drawbacks ranging from poor spatial coverage to temporal instability and low sensitivity. In-situ or field campaigns are the most accurate aerosol monitoring method but are significantly disadvantaged by the limited spatiotemporal range (Formenti et al., 2002; Ichoku et al., 2003; Smirnov et al., 2003). Meanwhile, in practice, remote sensing from both ground and satellite platforms constitutes the most commonly used method of aerosol measurement (Yakubu & Chetty, 2020). These methods are mainly advantageous due to their effectiveness in measuring the total column values of aerosol and non-intrusiveness (Smirnov et al., 2002). Besides, they possess considerably high stability in terms of temporal and spatial coverage. Although ground observation is still considered among the most effective remote form of observing aerosol properties. They are yet faced with the limitation of poor spatial coverage. Satellite-measured aerosol properties are less efficient, though they possess an uninterrupted temporal and broader spatial range (Sherman et al., 2016; Yakubu & Chetty, 2020). Therefore, ground and satellite remote sensing synergy for aerosol monitoring has demonstrated promising results (Kaufman et al., 2000). Also, modelled generated aerosol data is similarly stable temporally and spatially but prone to several errors since such data depends on in-situ, ground, and satellite data. Applying any or the synergy of these methods has helped characterised aerosol and investigate its impacts on climate (Schuster et al., 2012; Sherman et al., 2016; Yakubu & Chetty, 2020).

Natural and anthropogenic aerosols are often found as a mix globally. However, several studies have suggested that the increase in anthropogenic aerosols leads to the current challenge posed by climatic change (Charlson et al., 1992; IPCC, 2013; Schwartz et al., 2002). Also, findings have demonstrated that the aerosol suspension over an area is a function of both localised generated and in-ward transported aerosols from the external origin (Yakubu & Chetty, 2020). Hence, the characteristics of aerosol suspension can be predominantly influenced by localised generated aerosols or influx of transported aerosol particles. Meanwhile, some studies have shown that internally generated aerosols that mainly form a canopy over urban/industrialised environments emerge primarily from anthropogenic sources (Charlson et al., 1992; Schwartz et al., 2002; Wang et al., 2018). However, the occasional influx of transported aerosols also increases the aerosol suspended in some cases.

In contrast, rural and semi-urban areas are commonly dominated by natural aerosol emission but occasionally experience a sharp increment in aerosol suspension mainly due to the influx of transported particles (IPCC, 2007; Smirnov et al., 2003). Also, the mix of different aerosol suspensions has differing impacts on the corresponding region. Studies from various parts of the world have shown fine mode particles with generally absorbing characteristics and mainly originating from anthropogenic sources dominate the urban/industrial environments (IPCC, 2013; Yakubu & Chetty, 2020). The typical impact associated with this aerosol environment is an increase or decrease in the radiative forc-

ing (Twomey, 1977; Wang et al., 2018) due to the absorbing or scattering nature of the predominant particles, depending on the composition of the suspended aerosols.

Studies on urban/industrial regions such as America (Smirnov et al., 2003), Europe (Putaud, 2010; Sayer et al., 2014) and Central Asia (Wang et al., 2018) have shown that the impact of suspension due to urban/industrial aerosols on radiative forcing is a net warming effect (positive RF) following the strong absorption features of the constituents. Meanwhile, related studies in a similar setting elsewhere have shown the reverse (Yun et al., 2022). Polluted environments have also been presented to suppress precipitation formation (Fan et al., 2016; Rosenfeld, 1999). Nevertheless, some studies have found precipitation enhancement by high aerosol loading (Christensen & Stephens, 2012; Fan et al., 2016). Studies have consistently explained the two situations mainly to be influenced by atmospheric dynamics and thermodynamics (Fan et al., 2016; Rosenfeld et al., 2014). Over South Africa (SA), some studies have been carried out on characterising atmospheric aerosols suspended in the region. These include aerosol optical properties, the effect on radiative forcing, impacts on cloud and precipitation, and air pollution (Adesina et al., 2016; Formenti et al., 2002; Hersey et al., 2015; Ichoku et al., 2003). Generally, from those investigations, aerosols over SA exhibit seasonality centred around spring and aerosol loading is highest in the upper parts compared to the lower areas (Adesina et al., 2016; Tesfaye et al., 2011; Yakubu & Chetty, 2020).

Similarly, these studies have shown that the upper parts are distinctly dominated by fine mode aerosol, while the lower parts are a mix of coarse and fine aerosols. The primary sources of aerosols identified by these studies are observed to depend on the level of industrialisation, population and other related human activities. Also, they are sometimes enhanced by seasonal influx of biomass burning aerosol from neighbouring communities.

Regarding spatial coverage, most studies have investigated aerosol activities in fewer locations based on ground data, such as AERONET (Kumar et al., 2017; Queface et al., 2011) and more multilocation studies using satellite instruments data (Adesina et al., 2016; Tesfaye et al., 2011). Meanwhile, the validation of satellite aerosol retrieval over SA remains minimal, and most studies conducted using ground instruments such as sun photometers are mainly single location-based observations. Hence, only a few studies (Hersey et al., 2015; Yakubu & Chetty, 2020) have examined the validation of satellite measurements over the region, which are limited to small spatial coverage and often involve selected parameters. With the growing industrialisation and population across the region, urban expansion calls for more climate actions. Hence, understanding aerosol properties and the accompanying impacts become essential. Besides, more studies are needed to validate satellite-retrieved and modelled generated data, considering the vast gap set by satellite-based predominated studies over the region. This approach will enhance the reliability of satellite-based observations in studying aerosol regionally and globally.

This work investigates aerosol optical characteristics and the consequential impacts on radiative forcing over two metropolises in South Africa with distinct industrial and population footprints. Each of the two study areas represents the upper and lower parts of the country, respectively, and is strategic to Southern Africa. Furthermore, the areas are host to AERONET sun photometers and boast relatively consistent data regarding availability amongst peers. The study explores the advantages of these two sites attributes (as mentioned above) to understand the aerosol characteristics and radiative effects of locally generated and inward-transported aerosols. The role of naturally emitted and anthropogenic aerosols over each environment and proxy location is examined. Equally important, data from two satellite instruments over the sites will be validated using the AERONET data. The results present a comprehensive insight into identifying the predominant types and sources of aerosols in South Africa and their effects on the region. Further, the study will assist in deciding on an appropriate measure to tackle the climate change issue. Also, this output portrays a significant advance towards optimising satellite retrieval of aerosol

measurements over Africa and enhancing the modelling of aerosols over the region. Subsequently, section two describes the data, sources, and general approach to this study. Sections three and four give the study's detailed results and general discussion. Finally, the summary and a brief conclusion of the outcomes of this work are presented in section five.

2 Data and Methods

2.1 Locations

This study focused on two strategic metros (Pretoria and Cape Town) in South Africa (SA), separated by ≈ 2000 km within the regions geographical space (see Figure 1). Cape Town (33.92° S, 18.42° E) is one of the largest metropolitan areas in SA, located in the southernmost and coastal part of the region. The area has a mountainous and hilly landscape, including the famous Table Mountain, a popular tourist site. Also, the environment is typically a marine environment due to the nearness to the coast of SA. Cape Town is home to several industrial and commercial activities and represents the economic centre of the Western Cape province. The area, with a population of over 2-million people, is involved in different light industrial and domestic activities that result in the emission of a considerable amount of aerosols. Aerosols such as SO_4, NO_3, black (BC) and organic carbons (OC) are typical of this location (Yakubu & Chetty, 2020). Some aerosol impacts in this area include increased air pollution, weather changes, and associated health implications. Between 2013 and 2015, the region experienced low rainfall and was potentially prone to drought (Yakubu & Chetty, 2020). Similarly, a slight rise in air pollution and poorer air quality are observed from 2014 to 2018 (Yakubu & Chetty, 2022, 2020).

Pretoria (25.75° S, 28.28° E) is in Gauteng province northeast of SA, with another metropolis, Johannesburg, known as the country's economic capital. Due to proximity, the neighbouring city's (i.e., Johannesburg) population and activities significantly influence this area. Pretoria, popularly known as the administrative domain of SA, is home to extensive industrial activities, particularly the heavy steel industries. Mining activities and the coal power plant around the area are also essential sources of aerosol emission. In the last two decades, the city has suffered climate change impacts such as heat waves, precipitation drops and drought (McBride et al., 2022; Sen Roy & Rouault, 2013). Considering the series of climate change related events observed in the environment, there is a need to understand the role of aerosol emission changes over the area to mitigate the possible re-occurrence of such negative influences effectively. Besides, this study will enhance the characterisation of aerosols regionally and globally.

2.2 Data

For a detailed understanding of the aerosol properties and their corresponding impacts, this study utilises data from ground and satellite platforms to arrive at the result presented. The ground observation data is from the AERONET (Aerosol Robotic Network) stations in both locations. AERONET is a ground-based network of sun photometers that monitors the near real-time global distribution of aerosol spectral optical thickness through direct sun collimated and sky radiance measurements. The radiometers within the network take measurements at eight spectral bands: 340 nm, 440 nm, 500 nm, 675 nm, 870 nm, 970 nm and 1020 nm. The direct sun radiation is measured in all eight spectra, while the sky radiation is obtained at four wavelengths (440 nm, 670 nm, 870 nm and 1020 nm). Furthermore, AERONET provides aerosol optical depth (AOD) measurement at seven spectral bands and a nominal uncertainty of ≈ ±0.01-0.02 (Eck et al., 2013; Holben et al., 1998). From the AOD measurements at two reference wavelengths, another vital parameter, the Angstrom exponent (AE or α), which gives insight into the size characteristics of aerosols, is obtained. Also, from the spectral deconvolution algo-

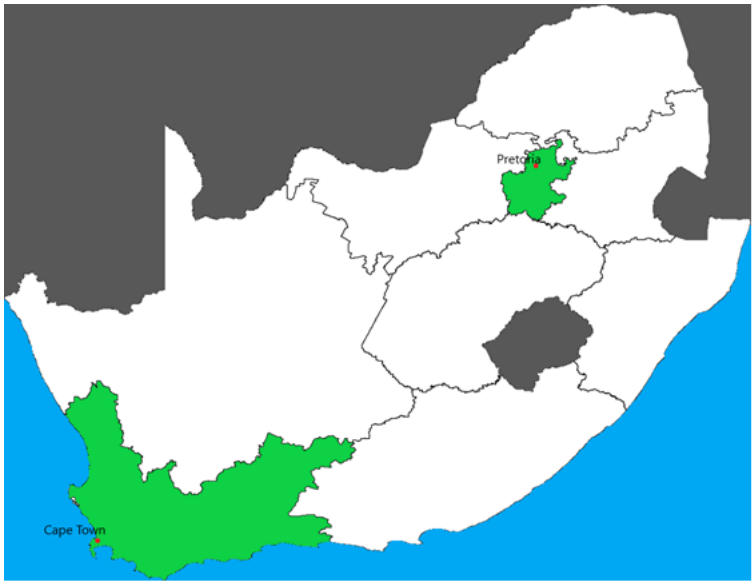

Figure 1. The map of South Africa showing the locations of Cape Town and Pretoria

rithm (SDA), properties such as the fine mode fraction (FMF) and AOD (τ_f) are inferred using the instrument measurements. Apart from the optical parameters, the network of radiometers produces microphysical parameters, including the volume size distribution, single scattering albedo (SSA), refractive indices (RI), and absorbing AOD (τ_{abs}), amongst others, using the flexible inversion algorithm and the sky radiance measurement as input (Dubovik & King, 2000). Several works have documented a detailed description of the retrieval method and products following the flexible inversion algorithm (Dubovik & King, 2000; Yakubu & Chetty, 2020). In this work, the level 1.5 scientific datasets from AERONET measurements for Pretoria and Simons Town sites to present the results herein. The preference for level 1.5 (cloud screen only) over level 2.0 (cloud screen and quality assurance) datasets is due to the size of datasets offered by the former and the consistency ($> 90\%$) compared to the latter, as observed from the two sites. Generally, the AERONET data is vital to this study as it provides an insightful view of aerosol optical and microphysical properties over the locations and validates satellite-derived data.

Both satellite data used in this study are measurements obtained from two instruments on board the Terra satellite, one of the A-train constellation satellites. The multiangle imaging spectroradiometer (MISR) instrument measures the reflected solar radiation from the earths surface by nine different cameras positioned at different angles; nadir, $\pm$ 26.1°, $\pm$ 45.6°, $\pm$ 60.0° and $\pm$ 70.5°, to monitor changes in global climate. Each of the nine cameras operates at four wavelengths; blue (443 nm), green (555 nm), red (670 nm) and infrared (865 nm) to provide various scientific datasets on aerosol and cloud properties beneficial for the proper characterisation of their impact on global climate. MISR possess the advantage of being carefully calibrated to operate at optimal accuracy to provide data at a high spatial resolution (Abdou et al., 2005; Diner et al., 1998; Kahn et al., 2010). Besides, the instrument offers the classification of aerosol particle size distribution among its peers. In the present study, level-3 daytime daily and monthly data at a spatial resolution of 0.5° x 0.5° are utilised to present additional results.

The moderate resolution imaging spectroradiometer (MODIS) has radiometric capabilities to measure the reflectance from clouds and the earths surface at 36 different spectrums ranging from visible to infrared. The instrument monitors the activities of aerosol and clouds at a horizontal resolution between 250 m and 1 km. MODIS produces different levels of aerosol products ranging from raw data (Level 1) to more refined datasets (Level 2 to Level 4). The higher-level aerosol products generally pass through further processing, where the datasets undergo different screening algorithms designated to filter-off inconsistent data. Also, a quality assurance (QA) flag is associated with successive product levels to enhance the quality of interpretation. Datasets from MODIS instruments form the basis of several studies, particularly over vast areas with no ground instruments. Hence, it is crucial to validate the data available from this instrument over all possible locations to assess the credibility in evaluating the past, present and future states of the atmosphere. Daily and monthly standard level 3, 1° x 1° gridded datasets are used for the analysis presented in this paper.

To evaluate the validation of the satellite retrieved data against the AERONET ground observation data, statistical metrics to include the correlation coefficient (R-value), significance value via 2-tail test (P-value), root mean square error (RMSE), mean average error (MAE) and the percentage mean bias (PMB) are considered. The identifications of the dominant aerosol types follow the application of an unsupervised clustering machine learning algorithm deployed using the Python Scikit module to corroborate the traditional identification process based on aerosol characteristics. Quantifying the direct radiative forcing (RF) due to aerosol in this work is based on the radiative transfer model. This model considers the difference in net fluxes (i.e., upward and downward fluxes) due to aerosol (without cloud) to estimate the RF at the top (TOA) and bottom (BOA) of the atmosphere. Thus, the average RF (ARF) over a region is typically esti-

mated as a function of RF at TOA and BOA following the expression below (Boiyo et al., 2019; Kumar et al., 2017);

$$ARF = RF_{TOA} - RF_{BOA}, \tag{1}$$

where,

RF_{TOA} = radiative forcing at the top of atmosphere

RF_{BOA} = radiative forcing at the bottom of atmosphere.

For this study, the RF at TOA ($RF^{'}_{TOA}$) and BOA ($RF^{'}_{BOA}$) derived from AERONET radiative forcing products are used. While the AERONET inferred $RF^{'}_{TOA}$ is used directly in equation (1) to account for net flux at TOA (i.e., $RF^{'}_{TOA}$= RF_{TOA}), $RF^{'}_{BOA}$ is applied to account for the downward net flux only. So, to represent the complete forcing at BOA to cater for the upward net flux, a correctional term as a function of the surface albedo ($\omega^{'}$) is applied to $RF^{'}_{BOA}$. Thus, RF_{BOA} in equation (1) is then expressed as;

$$RF_{BOA} = (1 - \omega^{'})RF^{'}_{BOA}. \tag{2}$$

Based on equation (2), the estimation of $\omega^{'}$ is done through the dataset of the MODIS albedo products. Thus, the level-3 MCD43A3 and the corresponding quality product (MCD43A1) are utilised to derive $\omega^{'}$ at the zenith ranging from 40° - 80° to account for changes in the instantaneous albedos (Wang et al., 2015).

3 Results

3.1 Aerosol optical properties statistics

The monthly averages of the parameters AOD, AE, FMF, AOD_{abs}, SSA and WVC over the study period 2015-2019 for Cape Town (CPT) and 2011-2019 for Pretoria (PRT) are presented in Figures 2 and 3. Generally, aerosol loading measured by AOD is lower in CPT (AOD_{av_440} = 0.08 ± 0.014), typical of the maritime environment (Smirnov et al., 2003), compared to PRT (0.23 ± 0.050), which boasts of more industrial activities, especially in the heavy metal industries. These observed values agree well with the reported ones from previous studies (Kumar et al., 2017; Yakubu & Chetty, 2020). Also, noticeably the two locations differ in the period of min-max occurrence of aerosol loading due to slight differences in climate patterns. Remarkably, the meteorological states are critical to aerosol characterisation owing to their roles in suspension and removal from the atmosphere. For instance, CPT is associated with the winter rainfall season resulting in the increase in aerosol removal by scavenging clouds ahead of the rainy events and is suggestively accountable for the minimum AOD (0.060) in April, as shown in Figure 2a, while the continuous suspension and the influx of air masses carrying aerosol is linked to maximum AOD (0.103) in August and most parts of spring.

Meanwhile, the case slightly differs for Pretoria, as illustrated by Figure 2b, such that the minimum AOD (0.159) occurred in June and the maximum (0.341) in September, extending through the spring season as seen for CPT and often associated with the events of biomass burning (BB) during the pre-farming season. Studies have repeatedly linked the BB events accounting for the high aerosol turbidity over the two locations in spring to mainly emanate from the northern parts of South Africa and neighbouring countries (Formenti et al., 2002; Hersey et al., 2015; Hodnebrog et al., 2016; Yakubu & Chetty, 2020). The concentration over each site is a function of the proximity and wind flux towards the area.

Following the characteristic aerosol loading over the study sites, CPT demonstrated the predominance of coarse particles (i.e., AE < 1.0) with a multiyear monthly average of 0.733 ± 0.128. At the same time, PRT tends more toward fine mode aerosols (i.e., AE > 1.0) with an average AE value of 1.517 ± 0.072. From Figure 2c, the minimum monthly mean AE (0.504 in March) and generally lower AE over Cape Town occur during the summer and autumn and coincide with the reduced influx of transported aerosol over the site. This variation significantly portrays the feature of a typical less polluted maritime environment with the predominance of sea salt (SS) aerosol. Previous studies over similar sites (de Leeuw et al., 2011; Smirnov et al., 2003), including this current site (Yakubu & Chetty, 2020), have demonstrated comparable variation and have been linked to a pristine coastal area predominated by coarse aerosol of SS origin. Similarly, the maximum monthly mean (0.929 in September) represents increasing aerosol loading dominated by finer particles and corresponds to the period of high atmospheric turbidity. This variation is associated mainly with the spring months, typically characterised by (internal and external) biomass burning and fossil fuel combustion. In contrast, aerosol suspension over Pretoria is chiefly dominated by fine mode aerosols (see Figure 2d). A mean monthly average AE (1.52) is recorded over PRT during the study period. Emissions from industrial activities, vehicular movements and other domestic activities are more likely to account for this variation. Meanwhile, the minimum AE (1.409 in July) and during the entire winter months suggest a decrease in fine particle dominated aerosols, such as BB aerosol, by relatively considering the drop in AOD value. The maximum (AE = 1.597 in December) and generally from spring to autumn indicates the enhanced emission and suspension of fine mode particles, influenced by the BB aerosol influx from external sources. This AE characteristic over PRT is consistent with the observation from a previous study over the site (Kumar et al., 2017).

The FMF variation from the spectral deconvolution algorithm (SDA) is presented in Figures 2e and 2f (i.e., for CPT and PRT, respectively) further to examine the particle size characteristics over the study sites. Coarse mode dominates atmospheric aerosol suspension over CPT, with FMF mostly less than 0.5 during most months of each season, such that the monthly average value (0.45 ± 0.056) reflects the dominance. This observation, coupled with the AOD and AE variation earlier described, strongly suggest SS as the primary aerosol type over the region. The minimum average FMF (0.360 in March) and low values in most months further display the strong dominance of SS aerosol over the area and less pollution. The maximum mean (0.542 in September) and relatively high values during winter signify increased pollution. These observations considerably align with the earlier findings in this work and the hypothesis from a previous study (Yakubu & Chetty, 2020), noting the influx of polluted air mass mainly linked to BB aerosol (i.e., aged smoke) from the northern part of South Africa. In contrast, FMF variation over PRT of a monthly mean value of 0.780 ± 0.029 illustrates the predominance of fine mode aerosol in the site. The minimum FMF (0.730 in November) represent the period of less influx of external air pollutant (especially aged smoke), while the maximum (0.821 in September) demonstrates the enhancement of internal air pollution due to the external influx of aerosol particles.

Figures 3a and 3b illustrate the variation of absorbing AOD (AOD_{abs} or τ_{abs}) over Cape Town and Pretoria, respectively. AOD_{abs} also constitute a vital property in aerosol characterisation and enhance the identification of different aerosol types. Aerosols such as carbon soot (CS) and black carbon (BC) are strong absorbers of solar radiation, hence, identifiable by high τ_{abs}. Low or relatively moderate τ_{abs} can infer moderately absorbing aerosols such as organic carbon (OC) and MD; those with poor absorbing properties are differentiable by extremely low AOD_{abs}. On this note, τ_{abs} is generally low over CPT (mean $\tau_{abs} = 0.005 \pm 0.002$) compared to PRT (mean $\tau_{abs} = 0.019 \pm 0.009$) with $\approx$ 4-times absorbing characteristics of CPT. The features presented by the AOD_{abs} variations in the two locations support the pattern demonstrated by AOD, AE and FMF. Also, the differences in τ_{abs} between the two sites beam more insight into the role of prox-

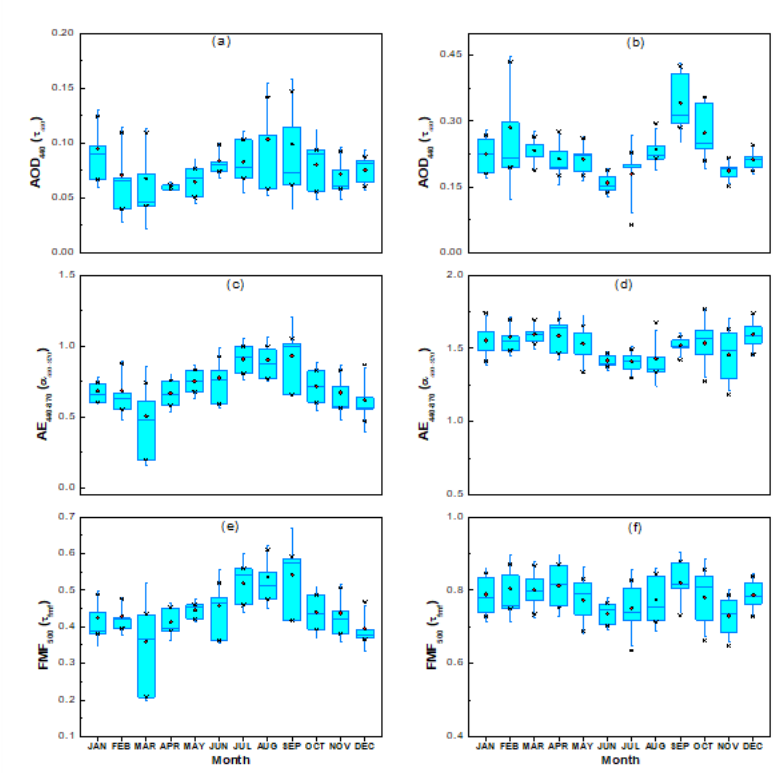

Figure 2. The graphs of the multiyear monthly mean AOD, AE and FMF for Cape Town; (a), (c) and (e), and Pretoria; (b), (d) and (f)

imity in the aerosol characteristics over each location. PRT is closer to the prime source of BB aerosols resulting in higher τ_{abs}, while CPT further away from the origin accounts for the lesser τ_{abs}.

Similar but opposite to τ_{abs}, the single scattering albedo (SSA or ω) variation over the study locations is described in Figures 3c and 3d for CPT and PRT, respectively. Over CPT, the monthly mean ω value is 0.932 ± 0.022 suggesting a considerable dominance of scattering suspensions. Factoring the variations portrayed by AOD, AE, FMF, and AOD_{abs}, the assertion of SS aerosols matching the predominant aerosol type over the Cape Town site is more apparent. The finding is consistent with the previous studies on the location (Yakubu & Chetty, 2020). Nevertheless, it is essential to note from the min-max SSA (i.e., 0.897-0.967) that aerosol suspended over this site sometime constitutes the mix of coarse-fine mode particles leading to characteristics shift in the value of SSA from strong to less scattering. Internal emissions such as domestic and industrial emissions and the influx of aged smoke-bearing air masses are often liable to these changes.

Similarly, the monthly mean ω in PRT is 0.899 ± 0.027, which chiefly represents scattering aerosols. However, compared with the obtained value over CPT, it demonstrates a more absorbing trait typical of an urban-industrial location and its proxy to the primary BB sources. The minimum average SSA (0.860) occurs in August, and the maximum value (0.948) is recorded in December. The minimum SSA and other lower values ($\omega < 0.890$) are chiefly associated with the winter and spring months, coinciding with the pre-planting period in South Africa and bordering countries. From the variations of SSA and other aerosol properties over Pretoria, one can observe the dominance of less absorbing and more scattering particles (like sulphate and nitrate aerosols) during autumn and summer. Likewise, the influence of less scattering and more absorbing aerosols (e.g., black and organic carbon) is observable around the winter and spring, thereby changing the spectral properties of the suspended particles.

Figures 3e and 3f illustrate the variations of atmospheric water vapour content (WVC) for CPT and PRT. WVC or precipitable water for both locations are similar in interpretation such that atmospheric vapour is lowest during winter (i.e., CPT;1.17 cm and PRT;0.67 cm, both in July) and highest in summer (CPT;1.99 cm in January and PRT;2.05 cm in December). This pattern is typical for all parts of South Africa, where WVC is all high during summer and lowest in winter. The monthly average WVC for the sites is 1.52 ± 0.29 cm and 1.35 ± 0.54 cm for Cape Town and Pretoria, respectively. Notably, the average WVC over CPT is higher than the value for PRT and is link-able to the nearness to the ocean since air temperature over the water drops slower compared to the land. Generally, the characteristics of high WVC during summer have been consistently reported over the hemispheres (Sioris et al., 2016; Yakubu & Chetty, 2022). Hence, the finding in this study is in good agreement with past studies.

Figures 4 and 5 show the validation of aerosol optical parameters data from the satellite (i.e., MISR and MODIS) observations over the locations under investigation against AERONET ground-measured data. In figures 4a and 4b representing Cape Towns MISR and MODIS AOD validations, respectively, one can see that the latter demonstrated better agreement with AERONET AOD following a moderate relationship (i.e., $R = 0.561$; $P << 0.001$) compared to the former with a very weak correlation (i.e., $R = 0.173$; $P = 0.466$). Also important, while MISR overestimated AOD over CPT by more than 50% relative to AERONET measurement, MODIS underestimated the parameter by approximately 10% (see Table 1 for complete metrics). Generally, both satellite instruments have been reported to retrieve AOD measurements over maritime/nearshore environments poorly (Kaufman et al., 1997). Several factors, such as the surface reflectance of water, instrument radiometric calibration, atmospheric correction and spatial resolution, are some of the sources of uncertainty in validating the two satellite instruments (Drury et al., 2008; Lora-Salazar et al., 2016). Although special algorithms are introduced in processing these datasets to correct and realign them with in-situ observation, environmen-

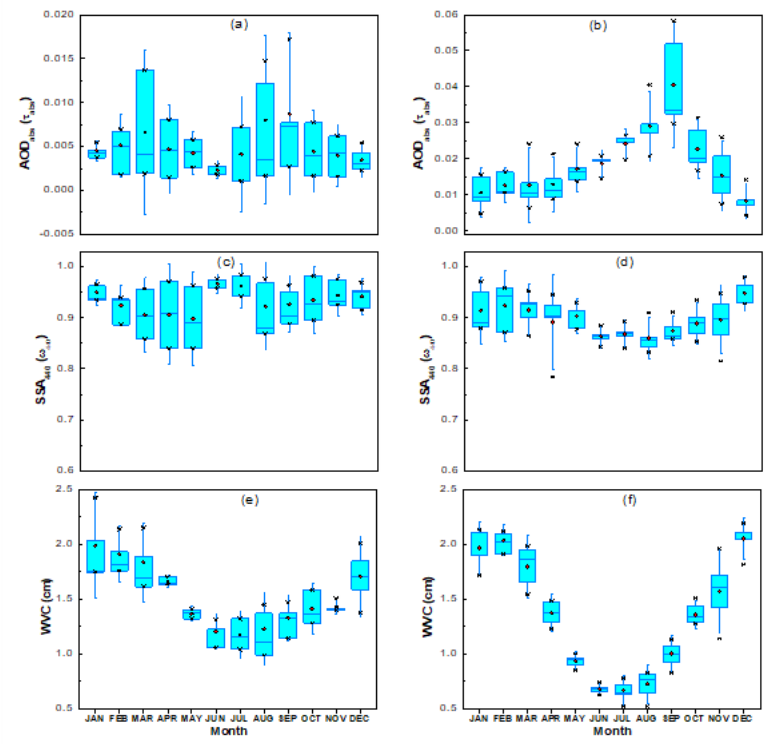

Figure 3. The plot of monthly mean AOD_{abs}, SSA_{440} and WVC for Cape Town; (a), (c) and (e), and Pretoria; (b), (d) and (f) over their respective study periods

Table 1. Summary of the statistical metrics adopted in the evaluation of the satellite validation

	CPT				
[a](M1 ; M2)	AOD	AE	AOD_{abs}	SSA	WVC
R-value	0.173 ; 0.561	0.069 ; 0.126	-0.033 ; 0.260	-0.014 ; -0.177	– ; 0.970
P-value	0.466 ; <0.001	0.773 ; 0.411	0.895 ; 0.105	0.960 ; 0.275	– ; <0.001
[b]Diff.(%)	50.08 ; -10.35	40.70 ; 103.42	13.84 ; -7.80	1.130 ; 0.590	– ; 0.570
RMSE	0.061 ; 0.026	0.380 ; 0.772	0.006 ; 0.004	0.061 ; 0.04	– ; –
MAE	0.050 ; 0.020	0.314 ; 0.753	0.005 ; 0.003	0.047 ; 0.032	– ; –
[a](M1 ; M2)	PRT				
R-value	0.611 ; 0.641	0.025 ; 0.106	0.579 ; 0.420	0.507 ; 0.424	– ; 0.990
P-value	<0.001 ; <0.001	0.858 ; 0.388	<0.001 ; <0.001	<0.001 ; 0.003	– ; <0.001
[b]Diff.(%)	-13.11 ; -53.62	-5.160 ; -1.270	-32.91 ; -58.26	3.530 ; 3.250	– ; 7.740
RMSE	0.068 ; 0.133	0.367 ; 0.133	0.011 ; 0.015	0.045 ; 0.059	– ; –
MAE	0.052 ; 0.125	0.295 ; 0.104	0.008 ; 0.012	0.037 ; 0.046	– ; –

[a]M1 = MISR, M2 = MODIS. [b]Diff.(%) = Percentage difference.

tal differences can influence the outcome of CPT. Also, the gap between the MISR and MODIS datasets is associable with the scanty data by the former compared to the latter.

Over PRT in Figures 4c and 4d, the result seems similar as seen for CPT. MODIS AOD measurement (R = 0.641; P << 0.001) slightly outperformed MISR AOD (i.e., R = 0.611; P << 0.001) in PRT. As an important note, the instruments demonstrated better retrieval on land than the ocean, as seen from observation over maritime/nearshore environments like CPT. Meanwhile, both instruments underestimated AOD relative to AERONET measurement over PRT, with MODIS taking the lead (see Table 1). Further to the above observations, improvement in data points for MISR has significantly enhanced the extent of agreement with the AERONET dataset.

AE retrievals from the two instruments relative to AERONET obtained measurements in Figures 4e 4h generally indicate weak agreements for both locations. Yet, the retrieval over the land (PRT) tends to be better than the counterpart in the nearshore CPT. In Figures 4e and 4f for CPT, MISR demonstrated a weaker correlation (i.e., R = 0.069; P = 0.773) compared to MODIS (i.e., R = 0.126; P = 0.411), respectively. Similarly, PRT in Figure 4g MISR (R = 0.025; P = 0.858) displayed a poorer correlation than MODIS (R = 0.106; P = 0.388) in Figure 4h. While both instruments averagely overestimated AE in CPT (i.e., MISR = 40.71%; MODIS = 103.42%), they underestimated the quantity in PRT (MISR = 5.16%; MODIS = 1.27%). The broader biases demonstrated by the AE retrievals are more associable with the inherited uncertainties from the AOD at individual wavelength profiled in the evaluation. Similarly, the dis-similarity in the choice of reference wavelengths in evaluating AE for the collocated AERONET and satellite instruments could also interfere with the correlation divergence.

Studying the validation plots of AOD_{abs} for the satellite instruments over CPT illustrated in Figures 5a and 5b, shows retrieval from MISR (R = -0.033; P = 0.895) and MODIS (R = 0.26; P = 0.105) weakly correlated with AERONET values. As with the observed relationship for AOD in CPT, the poor correlation was generally recorded for both satellite instruments. Nevertheless, MODIS AOD_{abs} tends to agree better with AERONET. In Figures 5c and 5d, respectively, for Pretoria MISR and MODIS AOD_{abs}, a moderate

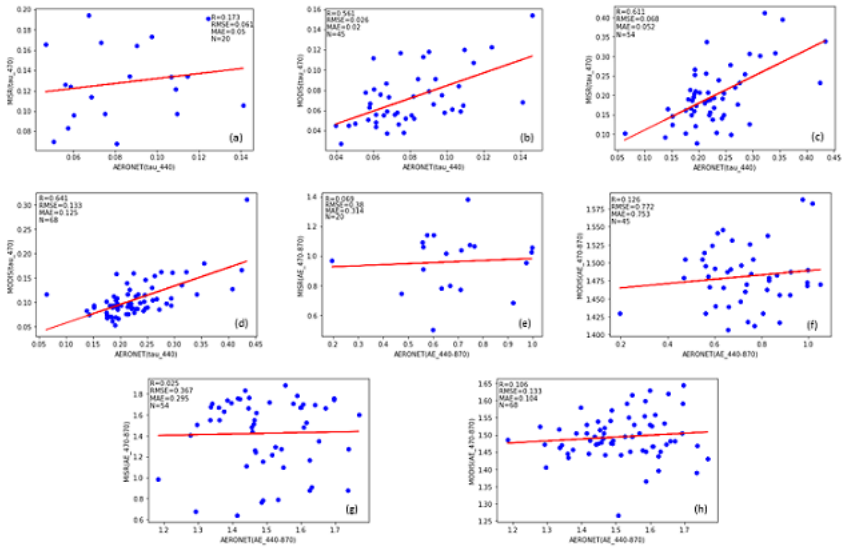

Figure 4. The plots of comparisons amongst AERONET, MISR and MODIS instrument data on AOD (a and b), AE (c and d), AOD_{abs} (e and f) and SSA (g and h) for CPT

correlation is observable for the two instruments compared to AERONET measurements. The MISR (R = 0.579; P << 0.001) demonstrated a more substantial relation with the ground instrument compared to MODIS (R = 0.42; P << 0.001). Overall, the trend of relatively better agreements of the satellite instruments with the collocated AERONET observation over the land surface is repeatedly demonstrated here for the AOD_{abs}, which is consistent with the earlier finding.

Comparison of SSA measurement between the satellites and ground instruments in Figures 5e-5h are similar to the relationship seen for AOD_{abs} over the locations. Weak connections between AERONET and the satellites SSA are recorded over CPT in which MISR (R = -0.014; P = 0.960) tends to be weaker than MODIS (R = -0.177; P = 0.275) measurement. Meanwhile, both satellite instruments posted a moderate relationship with the ground instrument in PRT, such that MODIS (R = 0.507; P << 0.001) is portrayed to be more assertive in correlation compared to MISR (R = 0.424; P = 0.003). Also essential, the satellite instruments averagely over estimated SSA measurement at both sites compared to the ground sensor, although by a minimal margin (i.e., < 4%). Further examining the satellite retrieval of another vital parameter available only from MODIS, the precipitable water, indicated robust agreement with the ground instrument in both locations. As expected, the accuracy over PRT (R = 0.99; P << 0.001) supersede that of CPT (R = 0.97; P << 0.001) and is accountable to the satellite instrument retrieval precision over land compared to the water surface. The WVC MODIS-AERONET relationship result obtained in this work consistently agrees with findings from previous studies (Kahn et al., 2010; Yakubu & Chetty, 2020, 2022).

3.2 Relationships amongst optical properties

In this section, the relationships AE vs AOD, SSA vs AOD, AE vs AOD_{abs} and aerosol index (AI) vs WVC are examined and presented in Figure 6 to further understand the aerosol characteristics over the study locations. AI represent a parameter de-

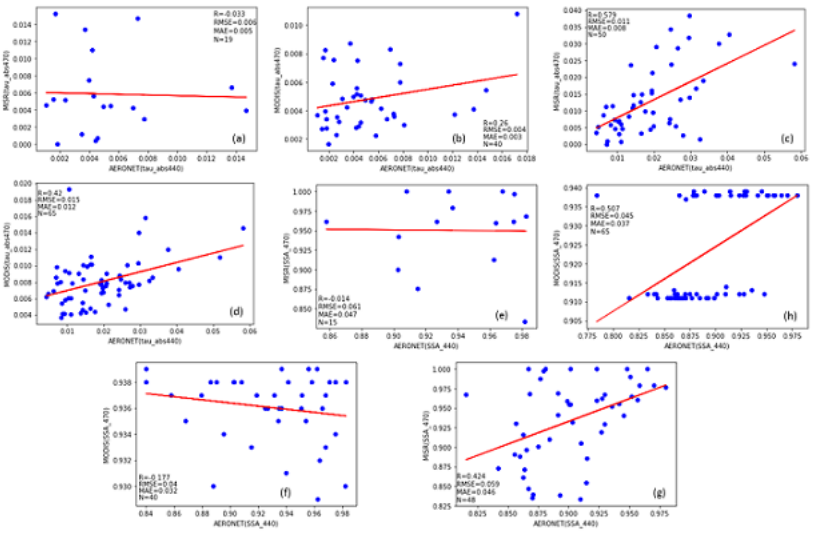

Figure 5. The plots of comparisons amongst AERONET, MISR and MODIS instrument data on AOD (a and b), AE (c and d), AOD_{abs} (e and f) and SSA (g and h) for PRT

fined as AOD *AE to factor the aerosol loading along with the size distribution in a single term. Figure 6a shows the relationship between AOD and AE for Cape Town. Mainly, low aerosol loading corresponds with large particle size (i.e., $\tau_{440} < 0.1$ primarily for $\alpha_{440-870} < 1.0$), then AOD between 0.1 and 0.15 consists of more mixed particle size (i.e., coarse and fine), and high atmospheric pollution over the location is dominated by fine-mode aerosols ($\tau_{440} > 0.15$; $\alpha_{440-870} > 1.0$). Similarly and more obviously, low aerosol loading over Pretoria is dominated by coarse-mode aerosols (i.e., $\tau_{440} < 0.1 \equiv \alpha_{440-870} < 1.0$), and high loading coincides with fine-mode particles ($\tau_{440} > 0.2 \equiv \alpha_{440-870} > 1.0$) as observed from Figure 6b.

The plot of SSA against AOD for CPT in Figure 6c demonstrates predominant scattering (i.e., $\omega > 0.9$) mainly for $\tau_{440} < 0.2$. The region of $\omega < 0.9$ coincides with $\tau_{440} > 0.2$ and the cluster of $\omega > 0.9$ lies with mostly high aerosol loading (i.e., $\tau_{440} > 0.15$). The first described region exhibits the characteristic of SS aerosols, the next is likened to carbon emission (including carbon soot, OC, and BC), and the last segment depicts sulphate and nitrate presence. These observations are consistent with the findings in the previous section and earlier study (Yakubu & Chetty, 2020), considering the environmental characteristics of CPT, such as the BB activities (including forest fire), the influx of aged smoke, and the level of industrial activities. For Pretoria in Figure 6d, again, the variation is more evident with the predominant spread of SSA > 0.9 extending from low to high aerosol loading (i.e., $0.15 < \tau_{440} < 1.20$) and the region of $\omega < 0.9$ for $0.15 < \tau_{440} < 0.90$. The first segment depicts the dominance of aerosols mostly from fossil fuel (FF) combustion (from domestic and industrial activities), such as sulphate and nitrate particles. The second part represents more mixed emissions from combustion activities (such as BB and FF) and mineral dust (MD). The characteristics of ω vs τ_{440} provide considerable evidence of CPT being SS rich, receiving low to moderate FF emissions and seasonally polluted by the combined internal and external low emissions from BB. In contrast, PRT demonstrates a significant suspension of sulphate and nitrate aerosols

through regular emissions from FF combustion and seasonally enhanced pollution by a large concentration of BB aerosol constituents (like BC, OC and soot).

The relationship between particle size and absorption strength for CPT in Figure 6e shows relatively higher τ_{abs} (> 0.02) are mainly influenced by fine-mode aerosols such as BC and OC. At the same time, the lower absorbing feature is associated with predominantly coarse mode aerosols suspected to be SS and considerable fine-mode concentration typical of FF combustion emission (sulphate and nitrate). In the case of PRT, aerosols of low absorption dominate the location. Thus, lower τ_{abs}-value mainly coincide with smaller-sized particles (AE > 1.0), and the same for $\text{AOD}_{abs} <$ with higher value ($\tau_{abs} > 0.04$). The first feature is typical of sulphate and nitrate aerosols, and the second is more of BC and soot. Meanwhile, the cluster of AE < 1.0 and $\text{AOD}_{abs} < 0.02$ comprises coarse non-absorbing aerosols, such as mainly MD considering the geographic location and the traces of SS aerosol.

Figures 6g and 6h illustrate the variation of AI with WVC for CPT and PRT. For CPT, increasing vapour content is accompanied by a moderate rise in the AI, especially for WVC values in the 1 to 2.5 cm range, which suggests growth in particle sizes due to water intake. Similarly, hygroscopic particle growth is evident for PRT following the rise in AI with WVC. This observation supports the evidence of the predominance of SS aerosols in CPT and sulphate-nitrate aerosol combination in the case of PRT, as depicted by the earlier figures (i.e., Figures 6a-6f).

3.3 Particle size distributions

The multiyear monthly average particle size distribution (PSD) for CPT in Figures 7a and 7b mainly displays bimodal characteristics that distinctly signify fine and coarse particles. Remarkably, the fine mode represents the region of radius (r) $< 0.4\mu$m and the coarse mode is marked by r) $< 0.4\mu$m. From the PSD variation in the figures, the coarse mode aerosol demonstrates a strong suggestion of predominance SS and possibly traces of MD. Several studies have shown that CPT is not prone to MD aerosol due to its general environmental characteristics, including not being within any desert regions proxies and possessing paved and tarred roads. However, the primary dust source is through occasional sedimentary weathering of rocks (Tesfaye et al., 2011; Yakubu & Chetty, 2020). The build-up of coarse mode volume concentration is observed in March and January, while a significant increase in fine mode particles notably occurred during July-September. These features are more apparent in the seasonal variation in Figure 7c, where distinct intensification of coarse mode particles is visible in summer, and peak concentration of fine mode aerosols is detectable in winter.

A substantial and distinct rise in the fine mode aerosol concentration (i.e., r $< 0.6\mu$m) is evident in February and September over PRT, thus demonstrating the predominance of fine particles as illustrated by the monthly average in Figures 7d and 7e. Additionally, several other peaks are observable in the region of r $> 0.6\mu$m, particularly for the months of May, June and September, as seen in the figures. These peaks represent the suspension of a significant amount of large-sized particles mainly due to the hygroscopic growth of hydrophilic aerosols (such as sulphate and nitrate) and emission from biomass burning activities (carbon soot), including from internal and external sources (i.e., considering the period of peak). This finding agrees well with the observation from several existing studies on the location (Adesina et al., 2016; Kumar et al., 2017; Yakubu & Chetty, 2022). Further to the monthly variation of PSD over PRT, Figure 7f displays the seasonal changes in the bimodal characteristics of the PSD. The highest concentrations of both coarse and fine mode aerosols are registered in spring, which depicts a scenario of mixed aerosol types linked to biomass burning and hydrophilic aerosols

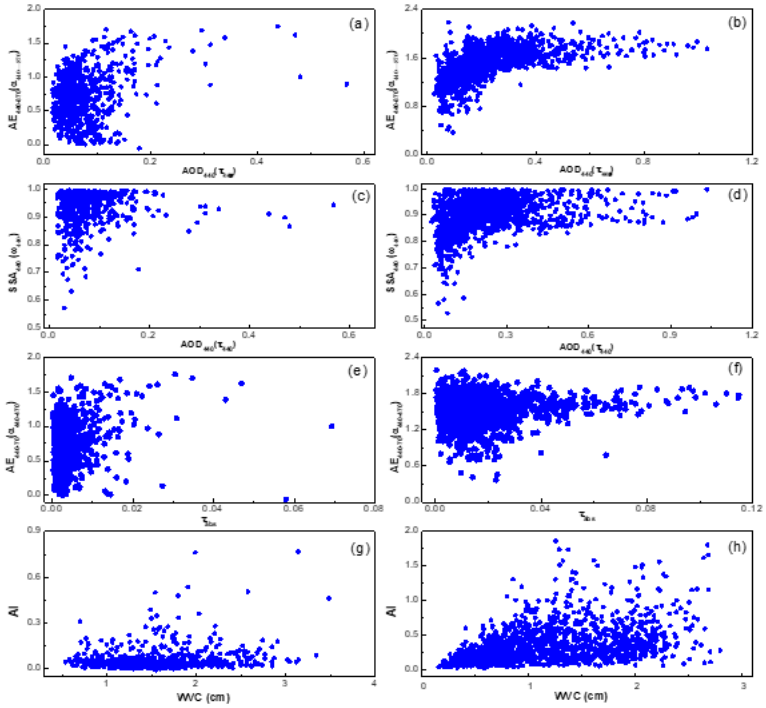

Figure 6. The plots of the relationships between AERONET, MISR and MODIS instrument measurement of the parameters AE vs AOD, SSA vs AOD, AE vs AOD_{abs} and AI vs WVC for CPT; (a), (c), (e) and (g), and PRT; (b), (d), (f) and (h)

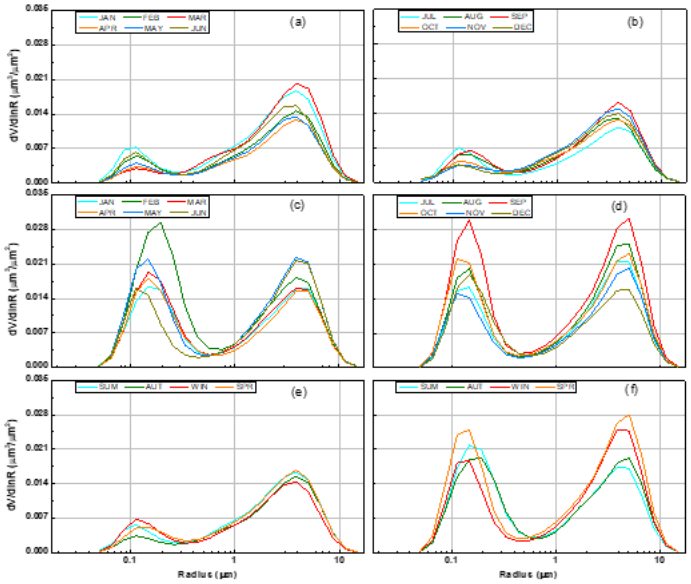

Figure 7. The illustration of monthly and seasonal average particle size distribution for CPT; (a), (C) and (e), and PRT; (b), (d) and (f))

3.4 Spectral Characteristics

The spectral behaviour of aerosol particles over the study locations is examined for wavelengths between 440-1020μm for AERONET, MISR and MODIS instruments. Figures 8a and 8b present the spectral characteristics of CPT and PRT, respectively. SSA in Figure 8a shows moderate spectral dependence such that ω is approximately steady between λ-values 440 and 680 nm, then slightly decreases with increasing wavelength at $\lambda > 680$ nm. This variation represents the mix of non-/absorbing aerosol typical for an urban-industrial setting that occasionally generates and receives an influx of absorbing particles like CPT. Meanwhile, the satellite observations of the spectral variation differ because both satellite instruments demonstrate increasing, then steady ω-values along with λ. The satellite observation from the MISR instrument follows the described pattern but approximately flattens as the wavelength changes. However, for MODIS, a strong spectral dependence of increasing ω with λ is visible for the few wavelengths range (i.e., 440-660nm) available for the instrument. Similarly, Figure 8b displays SSA exhibits moderate spectral dependence on wavelength, following ω sparingly decreasing with λ mainly at $\lambda > 800$ nm. The variation again indicates mixed-type aerosols of non-absorbing and absorbing properties which is consistent with the environmental situation of the PTR. MISR again exhibit closer similarity with the AERONET variation than MODIS, which is more divergent, just as experienced for CPT.

The variation of absorbing AOD for CPT illustrated in Figure 8c exhibits notable spectral dependency, mainly around $\lambda < 680$nm for the three instruments. An approximate steady value is noticeable for $\lambda > 680$nm. This variation shows the dominance of absorbing aerosol by fine particles and scattering aerosols by mainly coarse mode particles. The result from previous studies on this site has demonstrated similar variation (Yakubu & Chetty, 2020). Meanwhile, a strong spectral dependence is shown by AOD_{abs} over PRT in Figure 8d. AOD_{abs} decrease with increasing λ, and the pattern tends to be more evident at $\lambda < 680$nm. Like the pattern shown for CPT, smaller aerosol particles demonstrate higher absorption characteristics than larger ones. The AOD_{abs} spectral variation in PRT indicates a significant presence of absorbing fine mode aerosols such as BC and OC. Similar to the observation for CPT, the spectral characteristics of AOD_{abs} retrieved from MISR and MODIS instruments agree well with the AERONET measurement.

Apart from the spectral characteristics of ω and τ_{abs}, the refractive indices (i.e., the real and imaginary refractive index RI) also provide insights into the scattering and absorption properties of aerosol for possible identification of different aerosol types and size features. According to the trait exhibited by the real refractive index (RI_r) for CPT in Figure 8e, a significant change in the spectral behaviour of RI_r is observed such that it decreases with an increasing wavelength. This change is more apparent during the spring to autumn seasons. Since RI_r responds more to the scattering and particle size, the variation thus demonstrates the presence of a substantial amount of slightly large-sized absorbing aerosols (e.g., carbon soot). Further observation of the imaginary part of RI (RI_i) for CPT in Figure 8g, one can credibly notice an increase in absorption at $\lambda > 700$nm, which is consistent with the variation in Figure 8e. Thus, the average RI (RI_{av}) over CPT is 1.48 – i0.012, which is comparable to the RI of polluted urban marine environment (e.g., (Dubovik et al., 2002)).

In contrast, the RI_r for PRT in Figure 8f does not show strong spectral dependence as depicted by the RI_r for CPT, although the values (range 1.46-1.53) are higher than the observed values over CPT. These high values of RI_r are more evident for the winter and spring seasons associated with the intense emission of BB aerosol and particles from incomplete combustion of FF. Meanwhile, the lower values of RI_r for the other two seasons are liable to aerosol removal by increasing cloud developments and precipitation events. As for the RI_i in Figure 8h, the spectral dependence of RI with the wavelength is apparent at $\lambda < 650$nm and more associated with the winter and spring seasons. These

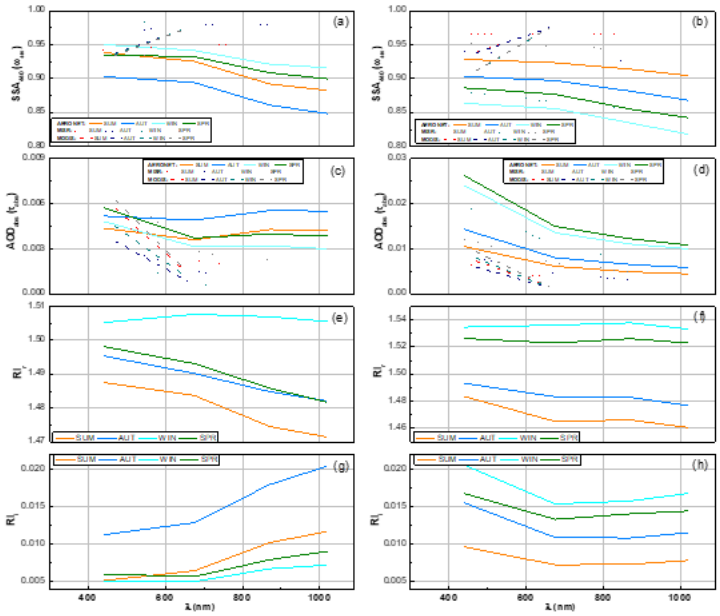

Figure 8. The graph showing the monthly and seasonal average spectral variation of SSA, AOD_{abs}, RI_r and RI_i for CTP (a, c, e and g) and PRT (b, d, f and h)

periods are primarily associated with increased fine mode absorbing aerosols mainly due to BB activities. Thus average RI_i for PRT decreases with λ, which with the variation of RI_r suggests the predominance of scattering aerosols. The mean RI over this site is 1.51 – i0.015, comparable to values recorded in BB polluted industrialised regions elsewhere (Dubovik et al., 2002).

3.5 Identification of the different aerosol types

After the aerosol properties examined in the previous sections, this section is intended to identify the prime aerosol types found in the locations under investigation. According to results from various existing studies (Boiyo et al., 2019; Giles et al., 2012; Smirnov et al., 2003), the behaviour of aerosol particles along the varying size range, absorption/scattering properties and the effect on light extinction constitute a vital and well-established method of inferring aerosol types. This is because different particle types differ in response to these attributes, although each feature cannot fully distinguish an aerosol type due to complex inter-similarities amongst particle types. Some studies have explored the methods of associating two or more properties to determine the different aerosol types in an environment (Boiyo et al., 2019; Kumar et al., 2017; Smirnov et al., 2003). However, these studies only consider particle size and aerosol loading or the size and absorbing/scattering characteristics. In this work, the particle effect on light extinction (AOD) and the absorption and scattering (ω and AOD_{abs}) are considered simultaneously to enhance the identification of the different aerosol types. The identification process mainly follows two

Table 2. Summary of the AOD, AOD_{abs} and SSA values associated with the different predominant aerosol types observed from the AERONET stations in (a) CPT and (b) PRT

(a)	Method I			Method II		
Type	τ range	τ_{abs} range	ω range	τ range	τ_{abs} range	ω range
SS	0.016 – 0.120	10^{-4} – 0.014	0.900 – 0.990	0.016 – 0.110	10^{-4} – 0.008	0.920 – 0.990
SO_4	0.140 – 0.570	10^{-4} – 0.024	0.920 – 0.994	0.080 – 0.234	$5x10^{-4}$ – 0.026	0.872 – 0.994
MD	0.016 – 0.140	0.002 – 0.021	0.800 – 0.900	0.016 – 0.171	0.001 – 0.031	0.827 – 0.930
OC	0.017 – 0.178	0.004 – 0.058	0.573 – 0.805	0.017 – 0.178	0.004 – 0.058	0.573 – 0.820
BC	0.150 – 0.480	0.016 – 0.069	0.840 – 0.913	0.279 – 0.480	0.019 – 0.069	0.850 – 0.937
(b)						
SS	0.032 – 0.090	$4x10^{-4}$ – 0.010	0.880 – 0.995	–	–	–
SO_4	0.080 – 0.379	$4x10^{-4}$ – 0.045	0.870 – 0.996	0.050 – 0.300	$4x10^{-4}$ – 0.049	0.810 – 0.996
MD	0.361 – 0.919	0.002 – 0.430	0.941 – 0.996	0.024 – 0.510	0.001 – 0.098	0.781 – 0.996
OC	0.037 – 0.370	0.005 – 0.078	0.527 – 0.870	0.026 – 0.250	0.002 – 0.065	0.527 – 0.980
BC	0.352 – 0.995	0.023 – 0.115	0.827 – 0.930	0.511 – 1.032	0.002 – 0.115	0.860 – 0.997

distinct procedures; (I) manual grouping of data points based on the scale of the three parameters under consideration and (II) application of clustering unsupervised machine learning (ML) algorithm using the three parameters as inputs.

Figure 9a shows the aerosol type classification based on AOD, ω and τ_{abs} for Cape Town using method (I). From the figure, five distinct clusters are identifiable. The cluster bounded by the red box represents the region of high scattering ($\omega > 0.89$), low aerosol loading ($\tau_{440} < 0.12$) and very low absorbing particles ($AOD_{abs} < 0.014$), which satisfy the features of SS aerosols and constitute the significant aerosol type over the site. The yellow box corresponding to high aerosol loading (AOD > 0.10), scattering ($\omega >$ 0.90) and low absorption ($AOD_{abs} < 0.02$) is linked to sulphate and nitrate aerosols. The orange box represents AOD < 0.02, 0.80 < ω < 0.90 and $AOD_{abs} < 0.02$ resembles more of MD. Also, the black box bounding particles with relatively low SSA ($\omega <$ 0.80), low to very high absorption, and AOD matches the carbonaceous soot and OC mix. At the same time, the cluster of AOD > 0.10, high absorbing and $\omega < 0.90$ (blue box) coincide with BC. Similarly, five distinct groups were detected using method (II) for CPT, as seen in Figure 9b. Generally, the clusters closely resembled those generated using method (I), although slight differences existed in boundaries defining each aerosol type. Table 2 fully describes detected boundaries defining the aerosol types obtained from both approaches.

Figure 10a illustrates the identification of the different dominating aerosol types over Pretoria based on the plot of AOD, SSA and AOD_{abs} using method (I). From the figure, the smallest cluster (red box) representing particles with high scattering and low absorption ($\omega > 0.9$, $AOD_{abs} < 0.02$ and AOD < 0.01) constitutes SS aerosols. The yellow box bounding high scattering aerosols with low absorption and AOD extending to high values matches sulphate and nitrate aerosols. Similarly, the region of high scattering (i.e.,$\omega > 0.92$), AOD ($\tau_{440} > 0.30$) and moderate to low absorbing feature (i.e., orange box) correspond to MD aerosols. Also, the cluster of particles having $\omega < 0.90$, low to moderate AOD_{abs}-values (i.e., 0.01 0.07), and AOD ranging from low to very high values bounded by the black box matches carbonaceous soot. Meanwhile, the segment of high absorbing, low scattering and high aerosol loading indicated by the blue box correspond to OC and BC mix.

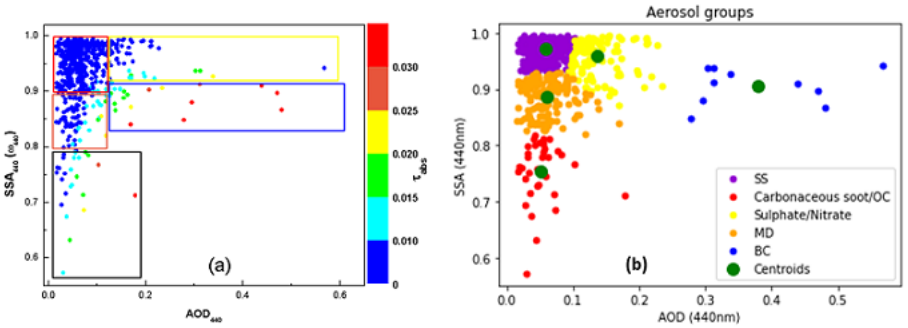

Figure 9. The cluster plot of different prime aerosol types based on the SSA, AOD and AOD_{abs} for CPT using procedure (a) I and (b) II

Unlike the output from method II for Cape Town that resulted in five distinct clusters similar to the pattern from its corresponding method I, four aerosol groups are detected for Pretoria using the machine learning approach. The identified clusters from method I substantially differ from those displayed by method II for the location, particularly around the region of AOD > 0.4 and high AOD_{abs}-values, as seen in Figure 10b. A summary of the identified clusters of crucial aerosol types is thus presented in Table 2. Hence from the identification process, sulphate and nitrate aerosols are the predominant aerosol types in the region which is consistent with the urban-industrialised characteristic of the location. Likewise significant is the identification of a substantial amount of carbonaceous aerosols (soot, OC and BC) being in suspension over the region and earlier suggested to result from local and external activities of BB. The results from aerosol observations and identifications for the two locations closely agree with several studies conducted over these sites and elsewhere globally (Boiyo et al., 2019; Kumar et al., 2017; Smirnov et al., 2003; Yakubu & Chetty, 2020).

3.6 Radiative forcing (RF)

A crucial impact of aerosol on the earth associated with huge uncertainties is the radiative forcing (RF) effect. The RF, which constitutes the primary factor that influences the global average temperature and is a critical climate driver, is a function of the amount of incoming shortwave (SWR) solar radiation and outgoing longwave (LWR) terrestrial radiation (IPCC, 2007, 2013). The effective RF mainly results in a net cooling effect when incoming SWR is lesser than outgoing LWR, a condition typical of predominated scattering aerosols. In contrast, a net warming effect occurs when SWR $>$ LWR, is mainly enhanced by absorbing particles (Kumar et al., 2017; Lohmann & Feichter, 2005).

Therefore, Figure 11 displays the multiyear average monthly RF at the bottom of the atmosphere (BOA), the top of the atmosphere (TOA) and ARF for Cape Town and Pretoria as observed from the AERONET instrument at each site. In Figure 11a, the

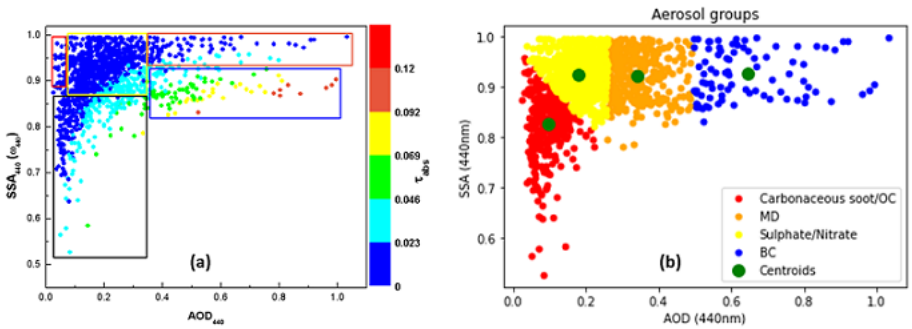

Figure 10. The cluster plot of different prime aerosol types based on the SSA, AOD and AOD_{abs} for PRT using procedure (a) I and (b) II

RF_{BOA} for CPT generally demonstrated a warming effect over the region with an overall average of 11.31 $\pm$2.01Wm^{-2}. The maximum monthly average of 14.50Wm^{-2} in September corresponds to the high aerosol loading period associated with the influx of aged smoke from BB activities outside the region. In comparison, the minimum 8.35Wm^{-2} in May coincides with the period of low aerosol loading. Similarly, for Pretoria in Figure 11b, a positive RF of a monthly average of 26.01Wm^{-2} is observed at the BOA leading to a warming effect. The maximum RF at BOA (45.55Wm^{-2}) recorded in September is linked to the activities of BB in the region and from boundary communities. Also, the peak coincides with the maximum over CPT, emphasising the drift of BB aerosol from the dominating sources in the north to the southern part of Southern Africa. Meanwhile, the minimum monthly value (18.97 Wm^{-2}) occurs in January and coincide with the period dominated by internally generated aerosols.

The RF at TOA depicts a negative forcing over CPT in contrast to the pattern shown by RF at BOA (see Figure 11a). The average monthly RF at TOA for the multiyear statistics is -5.34 $\pm$1.04Wm^{-2}, representing a cooling effect. From the chat, the maximum cooling effect (-6.49Wm^{-2}) occurs in September, while the minimum (-3.36Wm^{-2}) is recorded in March. For the PRT station (see Figure 11b), a similitude variation, as earlier seen in the case of CPT, is evident. A cooling effect with a multiyear monthly average value of -10.30 $\pm$1.91Wm^{-2} is observed at TOA over PRT. Meanwhile, the maximum negative RF at TOA is -14.20Wm^{-2} in February, and the minimum cooling effect is -7.56Wm^{-2}, which occurs in June. Therefore, the variation of RF at TOA demonstrated by both locations depicts the consequences of predominance scattering initiated by a differing factor such that coarse aerosol (SS) is linked to CPT, and fine particles (sulphate and nitrate aerosol) are associated with PRT.

According to the expression in equation (1), the effective RF (i.e., ARF) for the study locations, as shown in Figure 11 (a and b), apparently display net cooling effects (negative RF) over the two sites. Over CPT, an average net cooling effect of value -16.65

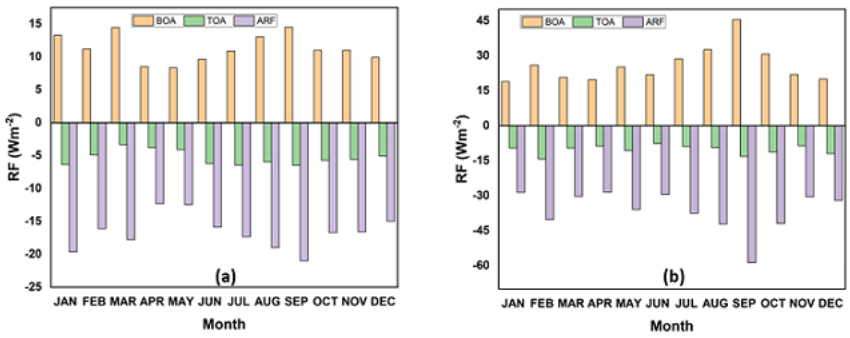

Figure 11. The graph of RF at BOA, TOA and average over CPT (a) and Pretoria (b)

$\pm 2.40 \mathrm{Wm}^{-2}$ is estimated over the location during the study period. The maximum cooling effect ($-20.99 \mathrm{Wm}^{-2}$) is attained during September, and the minimum ($-12.32 \mathrm{Wm}^{-2}$) is reached in April. Also, a net cooling effect averaged at -36.31 $\pm$8.36 Wm^{-2} in PRT during the study period. The monthly mean cooling effect at maximum ($-58.68 \mathrm{Wm}^{-2}$) occurs in September, coinciding with the month of higher aerosol loading. And as expected, the minimum cooling effect ($-28.55 \mathrm{Wm}^{-2}$) occurred during January, which is identified for low AOD. One can see that the net RF over the two locations result in a practical cooling effect. The magnitude of cooling is higher over PRT than CPT and significantly depends on the aerosol loading and the predominance of aerosol types suspended over the regions.

4 Conclusion

The optical properties and the consequential radiative effect of aerosol are investigated in Cape Town (CPT) and Pretoria (PRT), two renowned metropolitans with distinct background aerosol types and commonly influenced by biomass burning (BB) activities from the northern part of South Africa. Apart from the background aerosol, they differ in meteorological and climate circumstances due to geographical stance and internal activities. Thus, the followings are deduced from the observations.

Cape Town is mainly characterised by low aerosol loading predominated by coarse particles identified as sea salt (SS). In contrast, Pretoria is found to experience high aerosol loading, largely fine mode particles ailing from different combustion activities (i.e., BB and fossil fuel combustion). Furthermore, the aerosol loading over the two metropolitans is frequently influenced by BB activities emitted north of South Africa, including PRT during the pre-farming season in September, which alters aerosols spectral and radiative properties over the locations.

Aerosol suspension over CPT and PRT mainly demonstrated strong scattering characteristics and low absorption properties. While CPTs high scattering and low absorp-

tion characteristics are linked to coarse mode aerosols of marine origin (SS aerosols), suspension over PRT is more of fine mode particles ascribed to sulphate and nitrate aerosols. Further, the aerosol absorption feature increases in both locations during the period identified for the predominance of BB activities, with the prevalence more obvious for PRT.

The columnal precipitable water increases sharply over the two locations during summer, representing more than 65% compared to the values during the other sea seasons. Also, the average value for WVC is slightly higher in CPT than in PRT. Cape Towns nearness to the ocean is accountable for its higher values than PRT.

Validation of satellite instrument measurements of aerosol parameters against the AERONET datasets shows considerable agreement. However, some parameters such as AE, AOD_{abs} and SSA demonstrated poor agreement and large uncertainty regarding the ground instrument for specific locations and different platforms. On a general note, MODIS outperformed MISR in retrievals of most parameters and provided an exceptional dataset of atmospheric vapour measurement (i.e., for WVC, $R > 0.95$), which is unavailable for MISR. Considering the two locations, the satellite retrieval possesses better accuracy in PRT (mainly land surface) than for CPT (water environment).

Analysis based on the optical and spectral characteristics of the parameters under consideration (SSA, AOD_{abs}, RI_r and RI_i), the ranking of prominence aerosol types suspended over CPT follows the hierarchy MD < OC < BC < sulphate/nitrate < SS. Similarly, for PRT, the order of prominence follows SS < MD < OC < BC < sulphate/nitrate aerosols. Also, machine learning techniques demonstrate the capability to classify and identify different aerosol types based on their optical features.

The effective radiative forcing over the two locations is negative, resulting in net cooling effects and primarily influenced by different aerosol types in each case. Over CPT, the predominance of SS aerosols is observed to be responsible for this condition. In contrast, the prevalence of sulphate/nitrate aerosols is identified as the culprit for the net cooling effect over PRT.

Open Research Section

The datasets used in presenting the result in this work are obtainable from: https://www.aeronet.gsfc.nasa.g
bin for AERONET, https://www.asdc.larc.nasa.gov/data/MISR for MISR, https://www.ladsweb.modaps.eosdis.n
for MODIS and https://www.lpdaac.usgs.gov/products/mcd43a1v061 for MODIS albedo products only.

Acknowledgments

The authors wish to acknowledge the principal investigators of the AERONET sites in Pretoria and Simonstown for making the data available. The are also thankful to the MISR and MODIS team and their respective data distribution archive centre for the efforts toward making these scientific data available.

References

Abdou, W. A., Diner, D. J., Martonchik, J. V., Bruegge, C. J., Kahn, R. A., Gaitley, B. J., ... Holben, B. (2005). Comparison of coincident multiangle imaging spectroradiometer and moderate resolution imaging spectroradiometer aerosol optical depths over land and ocean scenes containing aerosol robotic network sites [Journal Article]. *Journal of Geophysical Research*, *110*(D10). doi: 10.1029/2004jd004693

Ackerman, A. S., Toon, O. B., Stevens, D. E., Heymsfield, A. J., Ramanathan, V., & Welton, E. J. (2000). Reduction of tropical cloudiness by soot [Jour-

nal Article]. *Science*, *288*(5468), 1042-1047. Retrieved from https://science.sciencemag.org/content/sci/288/5468/1042.full.pdf doi: 10.1126/science.288.5468.1042

Adesina, A. J., Kumar, K. R., & Sivakumar, V. (2016). Aerosol-cloud-precipitation interactions over major cities in south africa: Impact on regional environment and climate change [Journal Article]. *Aerosol and Air Quality Research*, *16*(1), 195-211. Retrieved from https://doi.org/10.4209/aaqr.2015.03.0185 doi: 10.4209/aaqr.2015.03.0185

Boiyo, R., Kumar, K. R., Zhao, T., & Guo, J. (2019). A 10-year record of aerosol optical properties and radiative forcing over three environmentally distinct aeronet sites in kenya, east africa [Journal Article]. *Journal of Geophysical Research: Atmospheres*, *124*(3), 1596-1617. doi: 10.1029/2018jd029461

Boucher, O. (2015). *Atmospheric aerosols: Properties and climate impacts* (1st ed.) [Book]. Netherlands: Springer. Retrieved from https://www.springer.com/gp/book/9789401796484 doi: 10.1007/978-94-017-9649-1

Charlson, R. J., Schwartz, S. E., Hales, J. M., Cess, R. D., Coakley, J., J. A., Hansen, J. E., & Hofmann, D. J. (1992). Climate forcing by anthropogenic aerosols [Journal Article]. *Science*, *255*(5043), 423-30. Retrieved from https://www.ncbi.nlm.nih.gov/pubmed/17842894 doi: 10.1126/science.255.5043.423

Christensen, M. W., & Stephens, G. L. (2012). Microphysical and macrophysical responses of marine stratocumulus polluted by underlying ships: 2. impacts of haze on precipitating clouds [Journal Article]. *Journal of Geophysical Research-Atmospheres*, *117*(D11203). Retrieved from <GotoISI>://WOS:000304766700003 doi: ArtnD1120310.1029/2011jd017125

de Leeuw, G., Andreas, E. L., Anguelova, M. D., Fairall, C. W., Lewis, E. R., O'Dowd, C., ... Schwartz, S. E. (2011). Production flux of sea spray aerosol [Journal Article]. *Reviews of Geophysics*, *49*(2). doi: 10.1029/2010rg000349

de Meij, A., & Lelieveld, J. (2011). Evaluating aerosol optical properties observed by ground-based and satellite remote sensing over the mediterranean and the middle east in 2006 [Journal Article]. *Atmospheric Research*, *99*(3-4), 415-433. doi: 10.1016/j.atmosres.2010.11.005

Diner, D. J., Beckert, J. C., Reilly, T. H., Bruegge, C. J., Conel, J. E., Kahn, R. A., ... Verstraete, M. M. (1998). Multiangle image spectroradiometer (misr) instrument description and experiment overview [Journal Article]. *IEEE T. Geosci. Remote*, *36*, 10721087. doi: https://doi.org/10.1109/36.700992

Drury, E., Jacob, D. J., Wang, J., Spurr, R. J. D., & Chance, K. (2008). Improved algorithm for modis satellite retrievals of aerosol optical depths over western north america [Journal Article]. *Journal of Geophysical Research: Atmospheres*, *113*(D16). Retrieved from https://doi.org/10.1029/2007JD009573 doi: 10.1029/2007JD009573

Dubovik, O., Holben, B., Eck, T. F., Smirnov, A., Kaufman, Y. J., King, M. D., ... Slutsker, I. (2002). Variability of absorption and optical properties of key aerosol types observed in worldwide locations [Journal Article]. *Journal of the Atmospheric Sciences*, *59*(3), 590-608. Retrieved from https://journals.ametsoc.org/view/journals/atsc/59/3/1520-0469_2002_059_0590_voaaop_2.0.co_2.xml doi: https://doi.org/10.1175/1520-0469(2002)059⟨0590:VOAAOP⟩2.0.CO;2

Dubovik, O., & King, M. D. (2000). A flexible inversion algorithm for retrieval of aerosol optical properties from sun and sky radiance measurements [Journal Article]. *Journal of Geophysical Research: Atmospheres*, *105*(D16), 20673-20696. Retrieved from https://agupubs.onlinelibrary.wiley.com/doi/abs/10.1029/2000JD900282 doi: 10.1029/2000jd900282

Eck, T. F., Holben, B. N., Reid, J. S., Mukelabai, M. M., Piketh, S. J., Torres, O., ... Slutsker, I. (2013). A seasonal trend of single scattering albedo in south-

ern african biomass-burning particles: Implications for satellite products and estimates of emissions for the world's largest biomass-burning source [Journal Article]. *Journal of Geophysical Research: Atmospheres*, *118*(12), 6414-6432. Retrieved from https://agupubs.onlinelibrary.wiley.com/doi/abs/10.1002/jgrd.50500 doi: 10.1002/jgrd.50500

Falaiye, O., Yakubu, A., Aweda, F., & Abimbola, O. (2013). Mineralogical characteristics of harmattan dust in ilorin, sub-sahara africa [Journal Article]. *Ife Journal of Science*, *15*(1), 175-181. Retrieved from https://www.ajol.info/index.php/ijs/article/view/131411/121007

Fan, J., Wang, Y., Rosenfeld, D., & Liu, X. (2016). Review of aerosolcloud interactions: Mechanisms, significance, and challenges [Journal Article]. *Journal of the Atmospheric Sciences*, *73*(11), 4221-4252. doi: 10.1175/jas-d-16-0037.1

Formenti, P., Winkler, H., Fourie, P., Piketh, S., Makgopa, B., Helas, G., & Andreae, M. O. (2002). Aerosol optical depth over a remote semi-arid region of south africa from spectral measurements of the daytime solar extinction and the nighttime stellar extinction [Journal Article]. *Atmospheric Research*, *62*(1-2), 11-32. Retrieved from www.elsevier.com/locate/atmos doi: 10.1016/S0169-8095(02)00021-2

Gettelman, A., & Sherwood, S. C. (2016). Processes responsible for cloud feedback [Journal Article]. *Current Climate Change Reports*, *2*(4), 179-189. Retrieved from https://doi.org/10.1007/s40641-016-0052-8 doi: 10.1007/s40641-016-0052-8

Giles, D. M., Holben, B. N., Eck, T. F., Sinyuk, A., Smirnov, A., Slutsker, I., ... Schafer, J. S. (2012). An analysis of aeronet aerosol absorption properties and classifications representative of aerosol source regions [Journal Article]. *Journal of Geophysical Research: Atmospheres*, *117*(D17). Retrieved from https://agupubs.onlinelibrary.wiley.com/doi/abs/10.1029/2012JD018127 doi: 10.1029/2012jd018127

Hansen, J., Sato, M., & Ruedy, R. (1997). Radiative forcing and climate response [Journal Article]. *Journal of Geophysical Research: Atmospheres*, *102*(D6), 6831-6864. Retrieved from https://agupubs.onlinelibrary.wiley.com/doi/abs/10.1029/96JD03436 doi: 10.1029/96jd03436

Haywood, J., & Boucher, O. (2000). Estimates of the direct and indirect radiative forcing due to tropospheric aerosols: A review [Journal Article]. *Reviews of Geophysics*, *38*(4), 513-543. Retrieved from <GotoISI>://WOS:000165171200004 doi: Doi10.1029/1999rg000078

Hersey, S. P., Garland, R. M., Crosbie, E., Shingler, T., Sorooshian, A., Piketh, S., & Burger, R. (2015). An overview of regional and local characteristics of aerosols in south africa using satellite, ground, and modeling data [Journal Article]. *Atmospheric chemistry and physics*, *15*, 4259-4278. Retrieved from https://www.ncbi.nlm.nih.gov/pubmed/26312061https://www.ncbi.nlm.nih.gov/pmc/articles/PMC4547400/ doi: 10.5194/acp-15-4259-2015

Hodnebrog, ., Myhre, G., Forster, P. M., Sillmann, J., & Samset, B. H. (2016). Local biomass burning is a dominant cause of the observed precipitation reduction in southern africa [Journal Article]. *Nature Communications*, *7*(1), 11236. Retrieved from https://doi.org/10.1038/ncomms11236 doi: 10.1038/ncomms11236

Holben, B. N., Eck, T. F., Slutsker, I., Tanr, D., Buis, J. P., Setzer, A., ... Smirnov, A. (1998). Aeroneta federated instrument network and data archive for aerosol characterization [Journal Article]. *Remote Sensing of Environment*, *66*(1), 1-16. Retrieved from http://www.sciencedirect.com/science/article/pii/S0034425798000315 doi: https://doi.org/10.1016/S0034-4257(98)00031-5

Ichoku, C., Remer, L. A., Kaufman, Y. J., Levy, R. C., Chu, D., Tanr, D., & Holben, B. N. (2003). Modis observation of aerosols and estimation of aerosol radiative forcing over southern africa during safari 2000 [Journal Article]. *J.*

Geophys. Res., *108*(D13). doi: 10:1029/2002JD002366

IPCC. (2007, 2007). *The physical science basis. contribution of working group i to the forth assessment report of the intergovernmental panel on climate change* (Report). Cambridge University Press.

IPCC. (2013). *Climate change 2013: The physical science basis. contribution of working group i to the fifth assessment report of the intergovernmental panel on climate change* [Book]. Cambridge, United Kingdom and New York, NY, USA: Cambridge University Press. Retrieved from www.climatechange2013.org doi: 10.1017/CBO9781107415324

Jacobson, M. Z. (2001). Global direct radiative forcing due to multicomponent anthropogenic and natural aerosols [Journal Article]. *Journal of Geophysical Research: Atmospheres*, *106*(D2), 1551-1568. doi: 10.1029/2000jd900514

Kahn, R. A., Gaitley, B. J., Garay, M. J., Diner, D. J., Eck, T. F., Smirnov, A., & Holben, B. N. (2010). Multiangle imaging spectroradiometer global aerosol product assessment by comparison with the aerosol robotic network [Journal Article]. *Journal of Geophysical Research*, *115*(D23). doi: 10.1029/2010jd014601

Kaufman, Y. J., Holben, B. N., Tanr, D., Slutsker, I., Smirnov, A., & Eck, T. F. (2000). Will aerosol measurements from terra and aqua polar orbiting satellites represent the daily aerosol abundance and properties? [Journal Article]. *Geophysical Research Letters*, *27*(23), 3861-3864. Retrieved from https://agupubs.onlinelibrary.wiley.com/doi/abs/10.1029/2000GL011968 doi: 10.1029/2000gl011968

Kaufman, Y. J., Tanr, D., Gordon, H. R., Nakajima, T., Lenoble, J., Frouin, R., ... Teillet, P. M. (1997). Passive remote sensing of tropospheric aerosol and atmospheric correction for the aerosol effect [Journal Article]. *Journal of Geophysical Research: Atmospheres*, *102*(D14), 16815-16830. Retrieved from https://agupubs.onlinelibrary.wiley.com/doi/abs/10.1029/97JD01496 doi: 10.1029/97jd01496

Kumar, K. R., Kang, N., Sivakumar, V., & Griffith, D. (2017). Temporal characteristics of columnar aerosol optical properties and radiative forcing (20112015) measured at aeronets pretoria-csir-dpss site in south africa [Journal Article]. *Atmospheric Environment*, *165*, 274-289. doi: DOI10.1016/j.atmosenv.2017.06.048

Lohmann, U., & Feichter, J. (2005). Global indirect aerosol effects: a review [Journal Article]. *Atmospheric Chemistry and Physics*, *5*, 715-737. Retrieved from <GotoISI>://WOS:000227375000002 doi: DOI10.5194/acp-5-715-2005

Lora-Salazar, S. M., Holmes, H. A., Patrick Arnott, W., Barnard, J. C., & Moosmller, H. (2016). Evaluation of modis columnar aerosol retrievals using aeronet in semi-arid nevada and california, u.s.a., during the summer of 2012 [Journal Article]. *Atmospheric Environment*, *144*, 345-360. Retrieved from http://www.sciencedirect.com/science/article/pii/S1352231016306690 doi: https://doi.org/10.1016/j.atmosenv.2016.08.070

McBride, C. M., Kruger, A. C., & Dyson, L. (2022). Changes in extreme daily rainfall characteristics in south africa: 19212020 [Journal Article]. *Weather and Climate Extremes*, *38*, 100517. Retrieved from https://www.sciencedirect.com/science/article/pii/S2212094722000962 doi: https://doi.org/10.1016/j.wace.2022.100517

Pope, C. A., Burnett, R. T., Thun, M. J., Calle, E. E., Krewski, D., Ito, K., & Thurston, G. D. (2002). Lung cancer, cardiopulmonary mortality, and long-term exposure to fine particulate air pollution [Journal Article]. *JAMA*, *287*(9), 1132-1141. Retrieved from https://doi.org/10.1001/jama.287.9.1132 doi: 10.1001/jama.287.9.1132

Putaud, J. (2010). European aerosol phenomenology-3: Physical and chemical characteristics of particulate matter from 60 rural, urban, and kerbside sites across

europe [Journal Article]. *Atmospheric Environment*, *44*, 13.

Queface, A. J., Piketh, S. J., Eck, T. F., Tsay, S. C., & Mavume, A. F. (2011). Climatology of aerosol optical properties in southern africa [Journal Article]. *Atmospheric Environment*, *45*(17), 2910-2921. Retrieved from <GotoISI>://WOS:000291079300012 doi: 10.1016/j.atmosenv.2011.01.056

Rosenfeld, D. (1999). Trmm observed first direct evidence of smoke from forest fires inhibiting rainfall [Journal Article]. *Geophysical Research Letters*, *26*(20), 3105-3108. Retrieved from https://doi.org/10.1029/1999GL006066 doi: 10.1029/1999GL006066

Rosenfeld, D., Andreae, M. O., Asmi, A., Chin, M., de Leeuw, G., Donovan, D. P., ... Quaas, J. (2014). Global observations of aerosol-cloud-precipitation-climate interactions [Journal Article]. *Reviews of Geophysics*, *52*(4), 750-808. doi: 10.1002/2013rg000441

Sayer, A. M., Hsu, N. C., Eck, T. F., Smirnov, A., & Holben, B. N. (2014). Aeronet-based models of smoke-dominated aerosol near source regions and transported over oceans, and implications for satellite retrievals of aerosol optical depth [Journal Article]. *Atmospheric Chemistry and Physics*, *14*(20), 11493-11523. Retrieved from https://www.atmos-chem-phys.net/14/11493/2014/ doi: 10.5194/acp-14-11493-2014

Schuster, G. L., Vaughan, M., MacDonnell, D., Su, W., Winker, D., Dubovik, O., ... Trepte, C. (2012). Comparison of calipso aerosol optical depth retrievals to aeronet measurements, and a climatology for the lidar ratio of dust [Journal Article]. *Atmospheric Chemistry and Physics*, *12*(16), 7431-7452. Retrieved from https://www.atmos-chem-phys.net/12/7431/2012/ doi: 10.5194/acp-12-7431-2012

Schwartz, S. E., Harshvardhan, & Benkovitz, C. M. (2002). Influence of anthropogenic aerosol on cloud optical depth and albedo shown by satellite measurements and chemical transport modeling [Journal Article]. *Proc Natl Acad Sci U S A*, *99*(4), 1784-9. Retrieved from https://www.ncbi.nlm.nih.gov/pubmed/11854481 doi: 10.1073/pnas.261712099

Seinfeld, J. H., Bretherton, C., Carslaw, K. S., Coe, H., DeMott, P. J., Dunlea, E. J., ... Wood, R. (2016). Improving our fundamental understanding of the role of aerosol-cloud interactions in the climate system [Journal Article]. *Proc Natl Acad Sci U S A*, *113*(21), 5781-5790. Retrieved from https://www.ncbi.nlm.nih.gov/pubmed/27222566 doi: 10.1073/pnas.1514043113

Sen Roy, S., & Rouault, M. (2013). Spatial patterns of seasonal scale trends in extreme hourly precipitation in south africa [Journal Article]. *Applied Geography*, *39*, 151-157. Retrieved from https://www.sciencedirect.com/science/article/pii/S014362281200166X doi: https://doi.org/10.1016/j.apgeog.2012.11.022

Sherman, J. P., Gupta, P., Levy, R. C., & Sherman, P. J. (2016). An evaluation of modis-retrieved aerosol optical depth over a mountainous aeronet site in the southeastern us [Journal Article]. *Aerosol and Air Quality Research*, *16*(12), 3243-3255. Retrieved from https://doi.org/10.4209/aaqr.2015.09.0568 doi: 10.4209/aaqr.2015.09.0568

Sioris, C. E., Zou, J., McElroy, C. T., Boone, C. D., Sheese, P. E., & Bernath, P. F. (2016). Water vapour variability in the high-latitude upper troposphere part 2: Impact of volcanic eruptions [Journal Article]. *Atmospheric Chemistry and Physics*, *16*(4), 2207-2016. Retrieved from https://www.atmos-chem-phys.net/16/2207/2016/ doi: 10.5194/acp-16-2207-2016

Smirnov, A., Holben, B. N., Dubovik, O., Frouin, R., Eck, T. F., & Slutsker, I. (2003). Maritime component in aerosol optical models derived from aerosol robotic network data [Journal Article]. *Journal of Geophysical Research-Atmospheres*, *108*(D1). Retrieved from <GotoISI>://WOS:000181576800014 doi: Artn403310.1029/2002jd002701

Smirnov, A., Holben, B. N., Dubovik, O., O'Neill, N. T., Eck, T. F., Westphal, D. L., ... Slutsker, I. (2002). Atmospheric aerosol optical properties in the persian gulf [Journal Article]. *Journal of the Atmospheric Sciences*, *59*(3), 620-634. Retrieved from https://doi.org/10.1175/1520-0469(2002)059<0620:AAOPIT>2.0.CO;2 doi: 10.1175/1520-0469(2002)059⟨0620:AAOPIT⟩2.0.CO;2

Tesfaye, M., Sivakumar, V., Botai, J., & Mengistu Tsidu, G. (2011). Aerosol climatology over south africa based on 10 years of multiangle imaging spectroradiometer (misr) data [Journal Article]. *Journal of Geophysical Research: Atmospheres*, *116*(D20). Retrieved from https://agupubs.onlinelibrary.wiley.com/doi/abs/10.1029/2011JD016023 doi: 10.1029/2011jd016023

Twomey, S. (1977). Influence of pollution on shortwave albedo of clouds [Journal Article]. *Journal of the Atmospheric Sciences*, *34*(7), 1149-1152. Retrieved from <GotoISI>://WOS:A1977DP78800020 doi: Doi10.1175/1520-0469(1977)034⟨1149:Tiopot⟩2.0.Co;2

Wang, D., Jiang, B., Li, F., & Lin, W. (2018). Investigation of the air pollution event in beijing-tianjin-hebei region in december 2016 using wrf-chem [Journal Article]. *Advances in Meteorology*, *2018*, 1-12.

Wang, D., Liang, S., He, T., Yu, Y., Schaaf, C., & Wang, Z. (2015). Estimating daily mean land surface albedo from modis data [Journal Article]. *J. Geophys. Res.*, *120*(10), 4825-4841. doi: 10.1002/2015JD023178

Yakubu, A. T., & Chetty, N. (2020). Optical properties of atmospheric aerosol over cape town, western cape of south africa: Role of biomass burning [Journal Article]. *Atmsfera*, *34*(4), 395416. doi: 10.20937/52811

Yakubu, A. T., & Chetty, N. (2022). A decadal assessment of the climatology of aerosol and cloud properties over south africa [Journal Article]. *Atmos. Chem. Phys.*, *22*(17), 11065-11087. Retrieved from https://acp.copernicus.org/articles/22/11065/2022/ doi: 10.5194/acp-22-11065-2022

Yun, L., Yuan, W., Bowen, P., Jiaxi, H., Song, G., Misti, L., ... Renyi, Z. (2022). Formation , radiative forcing, and climatic effects of severe regional haze [Journal Article]. *Atmos. Chem. Phys*, *22*, 4951-4967. doi: 10.5195/acp-22-4951-2022